Signaling Switch of the Axon Guidance Receptor Robo3 during Vertebrate Evolution

Pavol Zelina, Heike Blockus, Yvrick Zagar, Amélie Péres, François Friocourt, Zhuhao Wu, Nicolas Rama, Coralie Fouquet, Erhard Hohenester, Marc Tessier-Lavigne, et al.

Pavol Zelina [1, 2, 3†], Heike Blockus[1, 2, 3†], Yvrick Zagar [1, 2, 3†], Amélie Péres [4, 5, 6], François Friocourt[1, 2, 3], Zhuhao Wu[7], Nicolas Rama[1, 2, 3], Coralie Fouquet[8], Erhard Hohenester[9], Marc Tessier-Lavigne[7], Jörn Schweitzer[10], Hugues Roest Crollius[4, 5, 6] and Alain Chédotal [1, 2, 3*]

Signaling switch of the axon guidance receptor Robo3 during vertebrate evolution.

1 INSERM, UMRS_U968, Institut de la Vision, Paris, F-75012, France.

2 Sorbonne Universités, UPMC Univ Paris 06, Institut de la Vision, Paris, F-75012, France.

3 CNRS, UMR_7210, Paris, F-75012, France.

4 Ecole Normale Supérieure, Institut de Biologie de l'ENS, IBENS, Paris, F-75005 France.

5 CNRS, UMR 8197, Paris, F-75005 France.

6 Inserm, U1024, Paris, F-75005 France.

7 The Rockefeller University, 1230 York Avenue, New York NY 10065, USA.

8 CNRS, UMR_7102, Paris, F-75005, France.

9 Imperial College London, Department of Life Sciences, London SW7 2AZ, UK.

10 Institute Biology I, University of Freiburg, D-79104, Freiburg, Germany

† These authors contributed equally

*correspondence to: alain.chedotal@inserm.fr

Summary

Development of neuronal circuits is controlled by evolutionarily conserved axon guidance molecules including Slits, the repulsive ligands for roundabout (Robo) receptors and Netrin-1 which mediates attraction through the DCC receptor. We discovered that the Robo3 receptor fundamentally changed its mechanism of action during mammalian evolution. Unlike other Robo receptors, mammalian Robo3 is not a high affinity receptor for Slits, due to specific substitutions in the first immunoglobulin domain. Instead, Netrin-1 selectively triggers phosphorylation of mammalian Robo3 via Src kinases. Robo3 does not bind Netrin-1 directly, but interacts with DCC. Netrin-1 fails to attract pontine neurons lacking Robo3 and attraction can be restored in *Robo3*$^{-/-}$ mice by expression of mammalian but not non-mammalian Robo3. We propose that Robo3 evolution was key to sculpting the mammalian brain by converting a receptor for Slit repulsion into one that both silences Slit repulsion and potentiates Netrin attraction.

Introduction

Most animal species are *Bilateria* (Haeckel, 1866): they have a bilateral symmetry, with a front and a rear, and dorsal and ventral sides. The central nervous system of all these species contains special types of neurons, called commissural neurons, which extend their axons in commissures across the longitudinal axis of symmetry (or midline) to connect to target neurons located on the opposite side. The appearance of novel commissural systems or the modification of existing ones has accompanied the emergence of key neurobiological features in vertebrate evolution, such as depth perception, hearing, lung-based breathing and limb-derived locomotion (Goulding,

2009). Therefore, while vertebrate brains share a common overall architecture, many neuroanatomical differences can readily be observed, as well as differences in their ability to perform specific tasks. For instance, the corpus callosum, which interconnects both hemispheres, and the corticospinal tract (CST), which connects the sensorimotor cortex to the hindbrain and spinal cord, are two commissural projections that only exist in mammals (Shim et al., 2012; Suarez et al., 2014).

To investigate how axonal wiring is established during development, several vertebrate and invertebrate models have been used, on the reasonable postulate that fundamental aspects of this process are likely to be shared among species (Goodman, 1994). In most *Bilateria*, specific sets of cells occupy the midline and express axon guidance molecules that regulate crossing (Chédotal, 2011; Dickson, 2002). Two sets of ligand/receptor pairs are crucial in this process: Netrin-1/DCC (Deleted in Colorectal Cancer) which mediate attraction of commissural axons towards the midline and Slit/Robo (Roundabout) which mediate repulsion of post-crossing axons away from the midline and prevent ipsilaterally projecting neurons from crossing it (Brose et al., 1999; Keino-Masu et al., 1996; Kennedy et al., 1994; Kidd et al., 1999; Kolodziej et al., 1996). Various molecular interactions between the two pathways allow for a fine-tuning between attraction and repulsion (Chédotal, 2011). Surprisingly, although these mechanisms are largely conserved among species, a DCC ortholog appears to be absent from the chicken genome (Phan et al., 2011) and the commissureless proteins, which are negative modulators of Slit/Robo signaling in the Drosophila nerve cord, might exist only in Diptera (Sarro et al., 2013). This suggests that commissural axon guidance mechanisms may be more diverse across species than previously appreciated.

In vertebrates, the divergent Robo family member Robo3 plays a key role in midline guidance. Robo3 is expressed by commissural axons of the mouse spinal cord and hindbrain before and during crossing of the ventral midline (the floor plate), and many commissures fail to develop in mice and humans lacking Robo3 (Jen et al., 2004; Marillat et al., 2004; Renier et al., 2010; Sabatier et al., 2004). Several Robo3 splice variants, including a secreted form, have been described in vertebrates (Yuan et al., 1999; Camurri et al., 2005; Chen et al., 2008; Colak et al., 2013). How Robo3 controls commissure development at a cellular and molecular level is incompletely understood. Expression of Robo3 on pre-crossing commissural axons has been proposed to repress Slit/Robo repulsion, thus allowing commissural axons to reach, enter and cross the ventral midline in response to Netrin-1 attraction – a mechanism that appears to contribute to commissure formation by neurons in the spinal cord and lateral reticular nucleus but not apparently in the inferior olivary nucleus (Di Meglio et al., 2008; Sabatier et al., 2004; Jaworski et al., 2010; Chédotal, 2011). In addition, during initial characterization of Robo3, the possibility was raised that Robo3 might also facilitate attraction by the floor plate, independently of Slit/Robo signaling (Di Meglio et al., 2008; Jaworski et al., 2010; Sabatier et al., 2004). Here, we provide direct evidence for such a role through evolutionary analysis of Robo receptors using structural and computational biology, evolutionary genomics, functional biochemistry, and embryology. Specifically, we show that unlike all other Robo receptors, including Robo3 receptors in non-mammalian vertebrates, mammalian Robo3 receptors do not bind Slit ligands with high affinity, due to the substitution of a few specific key residues in the Slit/Robo binding domain. Moreover, mammalian Robo3 forms a complex with DCC and is phosphorylated on a conserved tyrosine residue in the presence of Netrin-

1 (but apparently without binding it) and contributes to the attractive actions of Netrin-1. Rescue experiments in mice and gain-of-function studies in zebrafish confirm the functional uniqueness of mammalian Robo3 receptors compared to other vertebrate Robo3s.

Results

Unique structural features of the mammalian Robo3 Ig1 domain

The *Robo3* gene is a member of a family of 4 genes (*Robo1*, *2*, *3* and *4*) that emerged from a single *Robo* gene in an ancestor of vertebrates by tandem duplication, which was further duplicated during two whole genome duplications (WGD) prior to the vertebrate radiation, with subsequent losses (Figures 1A and 1B). Today, two copies of the tandem duplication exist in most vertebrate genomes, with the *ROBO1* gene located head-to-head with the *ROBO2* gene on human chromosome 3, while the same configuration can be observed for the *ROBO3* and *ROBO4* pair on human chromosome 11. In vertebrates, the extracellular portion of Robo3 contains 5 immunoglobulin (Ig) domains and 3 fibronectin type III repeats (FNIII), whereas 3 to 4 conserved domains (CC0-CC3) can be identified in its intracellular region (Yuan et al., 1999; Sabatier et al., 2004 ; Figure 1C). The analysis of hSlit2/hRobo1 co-crystals revealed that Slits primarily bind through their second leucine rich domain (D2) to the first Ig domain of Robo1 (Figure 1E; Morlot et al., 2007). Interestingly, in mouse and human, only 70-77% identity is observed between the Ig1 domains of Robo1/Robo2 and Robo3 proteins, whereas Robo1 and Robo2 are about 92% identical. By contrast, non-mammalian Robo3 Ig1 domains are 86-96% homologous to Robo1/2 from the same species (Figure 1C). This increased molecular divergence of the mammalian Robo3 Ig1 is suggestive of functional divergence. In line with this, molecular evolution

analysis of the Robo3 Ig1 domain shows a marked signal of positive selection in the mammalian branch (Figure 1D and Figure S1, Table S1 and Table S2). Importantly, previous studies had indicated that Slit binding to Robo3 was either weak or absent (Sabatier et al., 2004; Camurri et al., 2005; Mambetisaeva et al., 2005). The alignment of the Ig1 domains of vertebrate Robos indeed revealed that three amino acids, predicted to be essential for hSlit2 binding to hRobo1 (Asn88, Lys90 and Leu130; Morlot et al., 2007), are conserved in all vertebrate Robo1 and Robo2 and non-mammalian Robo3 sequences but substituted exclusively in mammalian Robo3 (Figures 1E, 1F, S1 and data not shown). In all mammalian species analyzed (Table S3), Robo3 Ig1 always contains a proline instead of Asn88, an arginine instead of a Lys90 and a proline instead of a Leu130. These substitutions appear unique to mammalian Robo3 proteins and were not found in any other bilaterian Robo receptors (Figures S1 and data not shown). Of note, the two proline residues are among the sites that show a signature of positive selection (Figure S1 and Table S2). These observations are compatible with an accelerated evolution of Robo3 in early mammals and suggest that Robo3 might have lost the capacity to bind Slits with high affinity and therefore might have a different mechanism of action.

Mammalian Robo3 proteins are not high affinity receptors for Slits

To test this hypothesis, binding assays were performed by applying human Slit1-, Slit2-, or Slit3-AP fusion proteins on COS-7 cells expressing the two main splice isoforms of mouse Robo3 (mRobo3A.1, and mRobo3B.2; Chen et al., 2008; Sabatier et al., 2004). The expression and cell surface localization of Robo3 receptors (wild-type or mutated) was verified by Western blot and cell surface biotinylation experiments (data not shown). Slit-AP fusion proteins did not show detectable binding

to cells expressing any of the mouse Robo3 isoforms, whereas they all bound strongly to cells expressing rat Robo1 or Robo2 proteins (Figures 2A and S2). hSlit2-AP also failed to bind to hRobo3A.1 (Figure S2).

To confirm that the three substitutions in Ig1, unique to mammalian Robo3, account for the distinct Slit-binding properties, we used site-directed mutagenesis to introduce these three mutations (N88P, K90R and L130P) into rat Robo1, alone or in combination, and performed binding with hSlit2-D2-AP. In COS cells, mutated Robo1 constructs were expressed at levels comparable to wild type Robo1 and properly targeted to the membrane as determined by cell-surface biotinylation (data not shown). Whereas Slit2-D2-AP bound to wild type Robo1 (Figure 2A), it completely failed to bind Robo1$^{N88P/K90R/L130P}$ and Robo1^{L130P} (Figures 2B, 2E). Slit binding to other Robo1 mutants was not affected (Figures S2 and not shown).

In non-mammalian vertebrates (zebrafish, *Xenopus* and chick), Slit2-D2-AP bound with high affinity to Robo3 as expected from the conservation of the Ig1 domain in these species (Figure 2C-2E and S2). High-affinity Slit2 binding was abrogated in zebrafish Robo3$^{N83P/K85R/L125P}$, Robo3^{N83P} and Robo3^{L125P} and in *Xenopus* Robo3$^{N85P/K87R/L127P}$, Robo3^{L127P} which carry the mammalian substitutions (Figures 2C, 2E and S2). Notably, Slit2 binding to mRobo3 could be conferred on mouse Robo3 carrying the three reciprocal mutations, Robo3$^{P84N/R86K/P126L}$ or a single mutation of the proline 126 to a leucine, its counterpart in other Robos (Figures 2B, 2E and not shown). These results identify Pro126 in mammalian Robo3 as a key residue responsible for the lack of high affinity Slit2 binding.

It was previously predicted that the active Robo receptors might be dephosphorylated (Bashaw et al., 2000). Accordingly, Slit2 induced a significant tyrosine dephosphorylation of zebrafish Robo3 expressed in COS cells (Figure 3A). By contrast, Slit2 did not modify the phosphorylation level of mouse Robo3, as expected from the lack of detectable binding (Figure 3A). The Ig1-mutated zebrafish Robo3, unable to bind Slit2 with high-affinity, was not dephosphorylated by Slit2 (Figure 3B). Strikingly, the Ig1-mutated mouse Robo3, which effectively binds Slit2, showed a higher phosphorylation level than wild-type Robo3 and was dephosphorylated by addition of Slit2 (Figure 3B). These results strongly support the hypothesis of a functional change in the Ig1 domain of the Robo3 protein before the mammalian radiation, which led to a loss of high-affinity Slit binding.

Netrin-1 phosphorylates mammalian Robo3 via Src kinases

We next assessed whether mammalian Robo3 could respond to midline guidance cues other than Slits. We focused on Netrin-1, as it was previously suggested that Robo3 might mediate an attractive response to midline cues in addition to counteracting a repulsive one (Di Meglio et al., 2008; Jaworski et al., 2010; Sabatier et al., 2004), since both mechanisms could help explain the lack of commissures in *Robo3*-deficient embryos. We did not detect significant binding of Netrin-1-AP to any vertebrate Robo3 receptors tested (Figure S3A). However, the tyrosine phosphorylation of mammalian Robo3 was significantly increased by application of Netrin-1 whereas the phosphorylation of a non-mammalian Robo3 receptor was unchanged in presence of Netrin-1 (Figure 3C). To further characterize this process, we identified the tyrosine residue in Robo3 that is phosphorylated in presence of Netrin-1. The cytoplasmic domains of all mammalian Robo3 receptors contain 10

conserved tyrosines. We found that substituting tyrosine 1019 in the CC0 domain for phenylalanine (Y1019F) led to a complete abolishment of Netrin-1 induced Robo3 phosphorylation (Figures 3D) although the cell surface expression of the mutated receptor was not affected (Figure S3B). By contrast, mutating the neighboring Y1002 (Y1002F) had no effect on Robo3 phosphorylation (Figure 3D). To identify the kinase involved, we used two different algorithms for phospho-motif identification to analyze the Robo3 cytoplasmic domain for consensus sequences targeted by tyrosine kinases (Amanchy et al., 2007; Blom et al., 1999). This analysis identified Y1019 as a potential target for Src family kinases. The pharmacological kinase profiling of Robo3 phosphorylation was facilitated by the use of mouse P19 carcinoma cells, which express high levels of endogenous Robo3 (Yuan et al., 1999) that is also phosphorylated on cytoplasmic tyrosines in presence of Netrin-1 (Figure 3E). To obtain pharmacological evidence supporting the involvement of Src-kinases in Robo3 phosphorylation, we used PP2, a common inhibitor of Src family kinases. PP2 abolished the tyrosine phosphorylation of mouse Robo3 induced by Netrin-1 (Figure 3E). A comparable phosphorylation decrease was observed with a second Src-family kinase inhibitor (designated LckI, 7-Cyclopentyl-5-(4-phenoxyphenyl)-7H-pyrrolo[2,3‑d]pyrimidin-4-ylamine) that exhibits better selectivity than PP2 over other cytoplasmic tyrosine kinases (Anastassiadis et al., 2011; Figure S3C). To distinguish between Src-family kinases and c-Abl, we tested an inhibitor allosterically targeting c-Abl (GNF2; Choi et al., 2009) and did not observe any effect on Robo3 phosphorylation in P19 cells (Figure S3D). Finally, we overexpressed wild type or dominant-negative c-Src (K295M; Sandilands et al., 2004; Twamley-Stein et al., 1993) in COS cells co-expressing mouse Robo3. We found that the presence of dominant-negative c-Src abolished Robo3 phosphorylation (Figure 3F), suggesting that Src

family kinases, and possibly c-Src and not c-Abl, are mediating the phosphorylation of mouse Robo3 phosphorylation on Y1019 induced by Netrin-1. Interestingly, Y1019 is conserved in all Robo receptors, from Drosophila to humans (Figure 3G). Taken together these data show that during evolution, mammalian Robo3 not only lost high-affinity binding to Slits but also acquired the ability to be phosphorylated in presence of Netrin-1, which presumably occurs indirectly *via* another Netrin-1 receptor(s) given the lack of high-affinity binding of Netrin-1 to Robo3 (Figure 3H).

Robo3 is in a molecular complex with DCC

Previous studies showed that DCC can form a complex with Robo1 (Stein and Tessier-Lavigne, 2001). Although mammalian Robo3 lacks the CC1 domain that was proposed to mediate the DCC/Robo1 interaction, we nevertheless tested if Robo3 and DCC receptors could also interact. We first performed co-immunoprecipitation studies using E14.5 mouse hindbrain extracts and found that DCC could be co-immunoprecipitated with Robo3 (Figure 4A). The specificity of the immunoprecipitated bands was confirmed by their absence when extracts from *DCC*$^{-/-}$ embryos or *Robo3*$^{-/-}$ embryos were used (Figure 4A). Quantification of immunoprecipitated Robo3/DCC proteins indicated that about 15% of DCC was bound to Robo3. However, an interaction was still observed in extracts from *Netrin-1*$^{-/-}$ embryos (Figure 4A), suggesting the ligand is not crucially important for basal complex formation. Robo3/DCC interaction was also detected in HEK293 cells co-transfected with DCC and Robo3 independently of addition of exogenous Slit-2 or Netrin-1 (Figures 4B and S4). Full-length DCC and a truncated Robo3, lacking its extracellular domain, could still interact (Figure S4). The DCC/Robo3 interaction was also maintained with a Robo3 construct lacking its third conserved cytoplasmic domain (CC3 domain; Figure S4). However, DCC failed to bind to a mutant Robo3 receptor lacking both CC2

and CC3 domains, suggesting that the DCC cytoplasmic domain might bind to the CC2 domain of Robo3 or between the CC2 and CC3 domains (Figure 4D). Next we generated a mutant DCC lacking its P3 domain (DCC-ΔP3) which mediates DCC binding to Robo1 (Stein and Tessier-Lavigne, 2001). DCC-ΔP3 was unable to bind to Robo3 (Figure 4C). Together these results show that Robo3 and DCC are in a receptor complex and that Netrin-1 binding to DCC can induce Robo3 phosphorylation (see discussion). Although the phosphorylation of zebrafish Robo3 is not modified by Netrin-1, we could co-immunoprecipitate it with zebrafish DCC in transfected 293 cells (Figure S4).

Robo3 is required for attraction of commissural neurons by the floor plate and Netrin-1

What could be the evolutionary selective advantage of the molecular switch in Robo3 ligand properties and its influence on commissural systems? During development Robo3 is expressed by all hindbrain and spinal cord commissural systems including precerebellar pontine neurons (PN), which project their axons across the floor plate as mossy fibers to granule cells in the contralateral cerebellum (Marillat et al., 2004). Interestingly, among vertebrates, PN neurons have been identified only in mammals and birds (Wullimann et al., 2011). In mammals, PN neurons arise dorsally in the rhombic lip (RL) and migrate in a compact stream (the so-called anterior extramural stream or AEMS (Altman and Bayer, 1987) across several rhombomeres before turning ventrally towards the floor plate (Figures 5A-C). In the mouse embryo, this migratory stream could be visualized between E15.5-E17.5 with markers such as the transcription factors Barhl1 or by GFP expression following *in utero* electroporation in E13.5 embryos (Figures 5A-5C). Using these tools, we found that in *Robo3*$^{-/-}$ embryos the first migration phase of *Barhl1*+ PN neurons was indistinguishable from wild type

(WT) mice (Figure 5D-5F). However, after the PN neurons passed the root of the trigeminal nerve and initiated the ventral turn, the leading processes of Robo3-deficient PN neurons turned dorsally, thereby preventing PN neurons from approaching the midline. PN migration defects were highly similar in *Netrin-1* KO mice (Figure 5G). Pontine neurons were also previously reported to be absent in *DCC*$^{-/-}$ embryos (Fazeli et al., 1997; Yee et al., 1999). GFP electroporation revealed that PN neurons were still present in the *DCC* KO, but that they did not reach the ventral midline (n=11/11 embryos; Figure 5H). However, unlike in the other two mutants, PN neuron migration was also perturbed during the first phase, with small chains of neurons leaving the main stream to migrate ventrally or dorsally, before the root of the trigeminal nerves (n=11/11 embryos; Figure 5H). Although the PN migration defects were more severe in the *DCC* KO than in the *Robo3* KO and in *Netrin-1* KOs, these data raised the possibility that both Robo3 and DCC are required to mediate the attraction of PN neurons after they initiated their ventral turn. Immunostaining for DCC in the *Robo3* KO showed that DCC was normally expressed by Robo3-deficient PN neurons (Figure 5I). In addition, there was no significant ($p > 0.05$, ns, n=3-5 for each genotype) difference in the cell surface expression (as measured by biotinylation) of either DCC in *Robo3*$^{-/-}$ embryos or of Robo3 in *DCC*$^{-/-}$ embryos (Figures 5J-L). This rules out the possibility that a down-regulation of DCC in *Robo3* KO could explain the lack of attraction of PN neurons in these mutants.

To determine more directly if Robo3 is required for attractive responses of PN neurons, lower rhombic lip explants from E14.5 embryos (from *Robo3*$^{+/-}$ inter-crosses and therefore containing *Robo3*$^{+/+}$, *Robo3*$^{-/-}$ and *Robo3*$^{+/-}$ embryos), electroporated with GFP at E13.5, were dissected and cultured in collagen gels next to E11.5 floor plate explants. In this

strategy, the only cells expressing GFP were pontine neurons (Figure 6). In wild type explants, many streams of GFP+ neurons migrated towards the floor plate (Figure 6A). Strikingly, although GFP+ neurons were observed migrating inside explants from *Robo3*$^{-/-}$ embryos, exit of these cells into the collagen gel, reflecting attraction by floor plate, was suppressed (Figures 6B, 6F and Supplemental Movie S1). Since Netrin-1 attracts PN neurons (Alcantara et al., 2000; Yee et al., 1999), RL explants were cultured next to aggregates of Netrin-1-expressing cells. In wild type explants, chains of Pax6+ PN neurons migrated towards Netrin-1 expressing cells (Figures 6C and 6D). By contrast, in the case of explants from *Robo3*$^{-/-}$ embryos, no migration was observed towards Netrin-1 expressing cells, even though these cells contained functional DCC on their surface (Figures 5, 6E and 6G). We also tested the response of DCC-deficient PN neurons to Netrin-1 (Figure S5). Whereas attraction of PN neurons towards Netrin-1 cell aggregates was observed in 95.2% of the explants from *DCC*$^{+/+}$ embryos (n=21; from 5 experiments), it was not observed in 96% of the explants from *DCC*$^{-/-}$ embryos (n=25; from 5 experiments). Therefore, as for *Robo3*$^{-/-}$ explants, PN neurons from *DCC*$^{-/-}$ rhombic lip explants failed to be attracted by Netrin-1, suggesting that both receptors together are important in mediating Netrin-1 dependent attraction of PN neurons. Robo3 is also broadly expressed in spinal cord commissural neurons and is required for spinal cord commissure formation (Sabatier et al., 2004). To examine whether Robo3 also regulates the effect of Netrin-1 on spinal cord commissural axons, we cultured explants of dorsal spinal cord from E11.5 *Robo3*$^{-/-}$ and control littermates. The robust outgrowth of commissural axons induced by Netrin-1 from wild type explants was significantly reduced - but not abolished - when explants from *Robo3*$^{-/-}$ mutant embryos were used (Figure 6H), consistent with a conserved role for Robo3 in regulating Netrin-1 responses in commissural neurons in the hindbrain and spinal cord.

Selective rescue of pontine neuron migration defects by mammalian Robo3

To confirm that mammalian Robo3 is functionally distinct from non-mammalian Robo3, we performed rescue experiments. We used either *Robo3* null mice or a *Robo3* conditional knockout line (*Robo3*^{lox} ; Renier et al., 2010) crossed to a *Wnt1::Cre* line in which drives Cre recombinase in pontine neuron progenitors (Di Meglio et al., 2013; Nichols and Bruce, 2006; Rodriguez and Dymecki, 2000). As in the full knockout, PN neurons were unable to reach the ventral midline in *Wnt1:Cre; Robo3*$^{lox/lox}$ embryos (Figure 7A). For rescue experiments, E13.5 embryos were unilaterally electroporated in the rhombic lip with plasmids encoding either mouse Robo3A.1 or zebrafish Robo3A.1, together with GFP and embryos were collected at E16.5-E17.5. Both constructs were expressed in electroporated PN neurons as shown by Robo3 immunostaining, *in situ* hybridization and Western blot analysis (Figure S6). In all *Robo3* mutant embryos electroporated with mouse Robo3A.1 (n=8/8) many Robo3+ PN axons crossed the floor plate (Figures 7A and 7B and Figure S6). Moreover, chains of electroporated PN neurons left the main migratory stream and reached the ventral midline. Barhl1 and Pax6 immunostaining showed that the distance separating the floor plate from the main stream of migrating PN neurons was significantly reduced on the electroporated (rescued) side as compared to the non-electroporated side (Figure S6). The average ratio of the PN-to-midline distances between the electroporated and non-electroporated sides was 0.55±0.05 s.e.m. (n=4 embryos) for rescued compared to 1.05±0.09, s.e.m. (n=5 embryos) for controls (t-test, P=0.00208). By contrast, Robo3-deficient PN neurons expressing zebrafish Robo3 were still deflected dorsally and their axons did not approach the floor plate (Figures 7C, 7D and S6, n=8/8 embryos; ratio 1.03±0.003, s.e.m. from 4 embryos). The fact that mouse

Robo3 but not zebrafish Robo3 can rescue midline attraction in *Robo3*-deficient PN neurons supports the model that Robo3 from mammalian and non-mammalian species are functionally distinct and not redundant in their mechanism of action in commissural neurons. In further support, the mutated Robo3 receptor lacking the CC2-CC3 domain and unable to interact with DCC failed to rescue midline turning (n=4/4; Figure S6). Likewise, *Robo3*$^{-/-}$ pontine neurons expressing the Robo3^{Y1019F} receptor failed to reach the midline and their leading process did not cross it (n=4/4; Figure S6). This validates the functional importance of the CC2-CC3 cytoplasmic region and the phosphorylation of tyrosine 1019 in mediating Robo3 attraction.

To further investigate the phenotypic effects of adding mammal specific substitutions to non-mammalian Robo3A.1 protein we made use of the zebrafish Mauthner (MA) cell model, a pair of large neurons that project a commissural axon across the midline (Korn and Faber, 2005). MA axons express Robo3 during crossing and fail to cross the midline in *Robo3* mutant fish (Burgess et al., 2009). We studied the effect of mis-expressing different zebrafish Robo3 protein variants (with or without mammalian-specific Slit-binding residue mutations) during MA axon guidance. For temporal control of Robo3 expression we used *hsp70l:zrobo3a.1*, *hsp70l:zrobo3a.1*^{L125P} and *hsp70l:zrobo3a.1*^{N83PK85RL125P} transgenic lines, which in addition expressed tdTomato as a marker upon heat shock treatment (Figure S7; see Methods). Expression of the various transgenic zebrafish Robo3 constructs was heat-induced at 18 hours-post fertilization (hpf) while MA axons are actively crossing the midline (Miyashita et al., 2004). Embryos were fixed at 72 hpf and MA axons were labeled by whole-mount immunohistochemistry using anti-3A10. Heat shock treatment did not affect midline crossing of MA axons in wild type controls or in *hsp70l:zrobo3a.1*^{L125P} and

hsp70l:zrobo3a.1^{N83PK85RL125P} embryos (Figures 7E, 7G and 7H). In contrast mis-expression of wild-type z*robo3a.1* resulted in extra midline crossing events of MA axons (Figure 7F). Quantification revealed that upon mis-expression of *zrobo3a.1*, 30% of the embryos analyzed (n=192) showed additional midline crossing events of either one or both MA axons. In contrast, additional MA axon crossing events were only rarely observed in wild type controls (1.5%; n=206 embryos) or in embryos expressing z*robo3a.1*^{L125P} (2.5 %, n=119 embryos) or z*robo3a.1*^{N83PK85RL125P} (2%; n=209 embryos). Our findings show that zebrafish Robo3a.1 promotes MA axon midline crossing and that mutating either L125P or N83P-K85R-L125P (to abolish high-affinity Slit binding) perturbs this function. Taken together, these observations support that Robo3 from mammalian and non-mammalian species have functionally distinct mechanisms of action

Discussion

Unique function of the mammalian Robo3 receptor in axon guidance

Our results suggest that a few mutations in the Ig1 domain of mammalian Robo3 contributed to switch its function from being a Slit receptor to being a component of an attractive Netrin-1 receptor mechanism, at least for pontine neurons and spinal cord commissural axons. This function appears to be in addition to the role of Robo3 in silencing Slit repulsion *via* Robo1 and Robo2, observed in the spinal cord and lateral reticular nucleus (Chen et al., 2008; Jaworski et al., 2010; Sabatier et al., 2004). In most invertebrates and vertebrates, Robo receptors control axon guidance at the midline of the nervous system by mediating axon repulsion upon binding Slit ligands (Brose et al., 1999; Hao et al., 2001; Kidd et al., 1999; Kidd et al., 1998). Accordingly,

many studies have shown that in *Robo* and *Slit* mutants, cells or axons invade or remain in territories they normally avoid or just cross, such as the CNS midline. Therefore, the absence of hindbrain and spinal cord commissural tracts in *Robo3* knockout mice (Marillat et al., 2004; Sabatier et al., 2004) and patients suffering from HGPPS (horizontal gaze palsy with progressive scoliosis; Jen et al., 2004) was an unexpected finding: why would fewer axons cross the floor plate if the purpose of Robo3 was to mediate repulsion and, if in its absence, Slit repulsion was reduced? In the spinal cord, the Robo3.1 isoform is only expressed in precrossing commissural axons (Chen et al., 2008; Colak et al., 2013) and precrossing commissural axons from *Robo3* knockout mice are repelled by Slit, unlike wild-type commissural neurons which are not (Sabatier et al., 2004). This led to the hypothesis that Robo3 does not act to mediate Slit repulsion but rather acts as a negative regulator of Slit/Robo repulsion in precrossing axons. That model was further supported by the significant rescue of midline crossing in the spinal cord and lateral reticular nucleus of *Robo1/2/3* compound knockouts (Di Meglio et al., 2008; Jaworski et al., 2010; Sabatier et al., 2004). However, such rescue in *Robo1/2/3* triple KO is not observed in inferior olivary axons (Di Meglio et al., 2008) or pontine neurons (P.Z and A.C unpublished data), suggesting that in at least some commissural neurons, Robo3 might function independently of other Robo receptors. During the initial study of *Robo3* knockout mice, the formal possibility was raised that, in addition to repressing Slit repulsion, Robo3 might function by contributing to midline attraction, as this possibility was also compatible with available data (Sabatier et al., 2004). Indeed, we show here that Robo3-deficient pontine neurons are unable to reach the ventral midline *in vivo* and that they are unresponsive to the attractive action of floor plate and Netrin-1 *in vitro*, thus suggesting that Robo3 is required for attraction of these neurons. Moreover,

through quantitative analysis of spinal commissural axon responses, we show that mammalian Robo3 also potentiates the response of these axons to Netrin-1. Thus, our results establish that mammalian Robo3 participates in mediating attractive responses, in addition to its role in repressing Slit repulsion in some cells.

Robo3's mechanism of action in non-mammalian vertebrates is still unclear mostly due the lack of animal models. However, the reduction of MA axon crossing in Robo3 *twitch/twice* mutant (Burgess et al., 2009), the MA axon recrossing phenotype after Robo3 mis-expression, and the analysis of dopaminergic axon guidance in Robo3/Robo2 (*astray)* double mutant fish (Schweitzer et al., 2013), support a model in which zebrafish Robo3, like mammalian Robo3, promotes midline crossing by counteracting Slit/Robo repulsion but does so by binding Slits in an obligate fashion. Robo3 could block Slit/Robo repulsion by binding to Robo1/2, by titrating Slit, or by acting on downstream components, among other hypotheses. Some commissures do persist in the hindbrain of the *twitch/twice Robo3* fish mutant (Burgess et al., 2009; Schweitzer et al., 2013) and the knock-down of *Robo3* in chick spinal cord commissural neurons results in complex midline phenotypes affecting pre and post-crossing commissural axons (Philipp et al., 2012), which appears different from what is seen in *Robo3* knockout mouse embryos where crossing was fully prevented (Chen et al., 2008; Sabatier et al., 2004). This suggests that in non-mammals, Robo3 might have various axon guidance activities outside midline crossing. This is reminiscent of the *Drosophila*, were the three Robo receptors (Robo1-3) all require Slits but have different functions in commissure formation: Robo1 prevents crossing, Robo2 promotes crossing and Robo3 does not influence crossing (Rajagopalan et al., 2000; Simpson et al., 2000; Spitzweck et al., 2010). This was attributed to differences in specific cytoplasmic domains in each Robo receptors. Although we showed that

Netrin-1 induces the phosphorylation of a conserved tyrosine residue (Y1019) in mammalian Robo3, our preliminary data suggest that mutating this tyrosine in zebrafish (Y1024F) Robo3 is not sufficient to abolish its basal phosphorylation. This residual phosphorylation of the zRobo3^{Y1024F} could stem from a tyrosine in CC1, which is absent in mammalian Robo3 (data not shown).

Mammalian Robo3 binds to DCC and is activated by Netrin-1

Our study shows that mammalian Robo3 is not a high affinity receptor for Slits. Results from previous studies were ambiguous but suggested that Robo3B, but not Robo3A, receptors could bind Slits, albeit with much lower affinity than Robo1 and Robo2 (Camurri et al., 2005; Mambetisaeva et al., 2005; Sabatier et al., 2004). This was puzzling as Robo3A and 3B have identical Slit-binding Ig domains (their differences are N-terminal of the Ig1 domain) and also because it is unclear whether Robo3B even has a signal peptide. We also note that Robo4 is now believed to be unable to bind Slits with high affinity, even though initial studies suggested that it did (Jones et al., 2008; Koch et al., 2011). Slit2-AP did not bind to mammalian Robo3 receptors in our cell-based assay, but bound tightly to non-mammalian Robo3 receptors, and we identified amino acid substitutions in the first Ig domain that are responsible for this distinction. We also identify amino acids in the first Ig domain of mammalian Robo3 that are required for high-affinity Slit binding to other Robos but that appear to have specifically changed during evolution in the mammalian branch, apparently under a regime of positive selection. This suggests that during vertebrate evolution, mammalian Robo3 lost the ability to bind Slits but also gained the ability to be phosphorylated by Netrin-1, possibly a crucial necessity to function in a chemoattractive receptor complex.

Although Netrin-1 can induce phosphorylation of mammalian Robo3 via Src kinases, it does not bind directly to Robo3. Rather, our results suggest that DCC is the Netrin-1 receptor that triggers Robo3 phosphorylation. First, the comparison of the PN migration deficits in *DCC* and *Robo3* KOs indicates that these receptors are not required for PN neurons to turn ventrally but that they are both essential to reach the floor plate. Moreover DCC interacts with Robo3 in co-immunoprecipitation assays, most likely via their P3 and CC2 cytoplasmic domains, and a Robo3 receptor unable to interact with DCC fails to rescue Netrin-1 attraction in *Robo3*$^{-/-}$ PN neurons. This suggests that in pontine neurons Robo3 and DCC may form a receptor complex for Netrin-1, with Netrin-1 binding to DCC and Robo3 acting as a signalling component. Precerebellar neurons, including pontine neurons, express other Netrin-1 receptors such as Unc5B and Unc5C (Ackerman and Knowles, 1998; Bloch-Gallego et al., 1999; Di Meglio et al., 2013; Keino-Masu et al., 1996; Kim and Ackerman, 2011; Leonardo et al., 1997). There is a premature migration towards the ventral midline of a subset of pontine neurons in *Unc5c* and *Unc5b* knockouts (Di Meglio et al., 2013; Kim and Ackerman, 2011) suggesting that Unc5B and Unc5C act as repulsive receptors in at least a subset of PN neurons. However, the distinct PN migration defects in *Robo3* and *Unc5* knockouts suggest that PN attraction towards Netrin-1 is not mediated by a Robo3/Unc5 complex. By contrast in DCC knockout mice, the ventral turning of PN neurons is perturbed, as is their attractive response to Netrin-1 (see also Yee et al., 1999). Together, these observations suggest that Robo3 might cooperate with DCC to mediate Netrin-1 attraction in PN neurons. The same is also presumably true in spinal commissural neurons, since DCC is required for outgrowth in response to Netrin-1 in the assay used here (Keino-Masu et al., 1996; Xu et al., 2014). The interaction

between Robo3 and DCC could either be direct or involve adaptor proteins such as Nck, which has been shown to interact with both DCC and Robo cytoplasmic domains (Fan et al., 2003; Li et al., 2002). We show here that zebrafish DCC and Robo3 can interact, suggesting that the different signaling properties of mammalian and non-mammalian Robo3 receptors in response to Netrin-1 are not due to a differential binding between DCC and Robo3. This is somehow expected as previous studies showed that Robo1 also binds to DCC in a Slit dependent-manner (Stein and Tessier-Lavigne, 2001) but that in this case, Robo1 silences Netrin-1/DCC-mediated attraction whereas DCC does not modulate Robo1. Although all Robo3 receptors contain three highly conserved cytoplasmic domains (CC0, CC2 and CC3) there is a high variability outside these domains. Moreover, mammalian Robo3 lack the CC1 domain presents in other Robo receptors. These differences probably account for the distinct responses to Netrin-1.

A role for Robo3 in the evolution of mammalian motor circuits?

A key event in the evolution of the nervous system in Eutherian mammals was the appearance of two major commissural systems, the corpus callosum and the corticospinal tract (CST)(Richards et al., 2004). CST axons convey motor outputs from the cortex to motor neurons, either directly, as in primates, or indirectly via interneurons, as in rodents (Canty and Murphy, 2008). During their descent to the spinal cord, CST axons send collateral branches to pontine neurons (Heffner et al., 1990; O'Leary and Terashima, 1988) in response to a still unidentified chemoattractant. This cortico-pontine projection allows a copy of motor commands to reach the cerebellum, which is essential for motor planning and the control of fine movements. Previous studies supported a correlated evolution of the cortex and cerebellum in mammals (Barton, 2012) but the anatomical

correlates were unknown. Our results suggest that a small number of adaptive mutations of Robo3 in mammals, leading to the formation of a ventral pontine nuclei, might have facilitated, through CST branches, the connection of the cortical motor system to the cerebellar system thereby improving the planning and learning of motor tasks in mammals. In vertebrates, pontine neurons have only been observed in mammals and birds (Wullimann et al., 2011). However, the anterior extramural migratory stream of pontine neurons has only been described in mammals, and preliminary experiments suggest that it does not exist in chick (A.C and P.Z unpublished data). The *in vivo* rescue experiments show that mouse PN neurons expressing non-mammalian Robo3 are not able to reach the floor plate. This suggests that the evolution of Robo3 in mammals might have allowed PN neurons to reach the floor plate, thereby placing them on the pathway followed by CST axons. Although spinal cord commissural neurons do not migrate to the floor plate, our explant cultures show that Robo3 potentiates the Netrin-1 response in this commissural system as well. Therefore, mutations of mammalian Robo3 might have also facilitated the ability of commissural axons to read the Netrin-1 gradient in larger brains. Of note, 12 additional sites in the mammalian Robo3 Ig1 domain appear to have undergone positive selection (Table S2) and were not characterized here. These may either participate in a non-critical way to the change in Slit repulsion described here, or may be involved in additional roles of the Robo1 Ig1 domain or binding with other Robo partners.

In conclusion, while much of the past analysis of axon guidance mechanisms has appropriately focused on their evolutionary conservation, our results illustrate how subtle adaptive changes in the sequence of an axon guidance receptor can lead to fundamental changes in its function and distinct neuronal circuits, helping to understand the

emergence of specific sensory, motor and cognitive functions and why they differ between species.

Experimental procedures

Analysis of Robo genes

We extracted the annotated protein and coding sequence (CDS) of *Robo1*, *Robo2* and *Robo3* in multiple vertebrate genomes from the Ensembl database (Flicek et al., 2014) and NCBI. Multiple alignments of the protein sequences were performed using T-Coffee (Notredame et al., 2000) and reverse-translated in a CDS multiple alignment using the corresponding *Robo* CDS sequences. Phylogenetic gene trees were constructed using the TreeBest pipeline (Vilella et al., 2009) and reconciled with the known species tree. To identify positive selection in Robo3, we compared the relative rates of synonymous and non synonymous substitutions ($\omega = dN/dS$) using the PAML package (Yang, 2007). The Branch-Site Model was used to test each branch separately. In this model, the ω ratio varies both among sites and among lineages, thus making it possible to detect positive selection that affects only a few sites along a few lineages. Models were evaluated using likelihood ratio tests (LRTs) and $\chi 2$ tests of significance. Sites with Bayes Empirical Bayes (BEB) scores higher than 0.5 were considered indicative of positive selection. We used ClustalW multiple alignments of Robo sequences to calculate identity percentage between Robo Ig1 domains.

Expression plasmids.

See Extended Experimental Procedures for origin and details of the plasmids used in this paper.

Mouse strains and genotyping

Netrin-1 (Serafini et al., 1996), *DCC* (Fazeli et al., 1997); *Robo3* (Sabatier et al., 2004) and *Robo3^{lox}* (Renier et al., 2010) knockout mice and the *Wnt1::cre* line (Rodriguez and Dymecki, 2000) were previously described and genotyped by PCR. The day of the vaginal plug was counted as embryonic day 0.5 (E0.5). Mice were anesthetized with Ketamine (100mg/ml) and Xylazine (10mg/ml). All animal procedures were carried out in accordance with institutional guidelines.

Zebrafish transgenesis

See Extended Experimental Procedures.

Immunohistochemistry

Collagen explants and mouse embryos (until E16) were fixed by immersion in 4% paraformaldehyde in 0.12M phosphate buffer, pH 7.4 (PFA) for 1 hour at room temperature (RT). Whole hindbrains and collagen explants were blocked in 0.2% gelatin in PBS containing 0.25% Triton-X100 for 2 hours RT, and incubated overnight at 4°C with rabbit anti-human Barhl1 (Sigma), goat anti-human Robo3 (R&D Systems), rabbit anti-mouse/human Pax6 (Chemicon) and mouse anti-beta-III-tubulin (TUJ1, Covance), followed by species-specific secondary antibodies directly conjugated to fluorophores (Cy-5, Cy-3, Alexa-Fluor from Jackson ImmunoResearch, West Grove, PA or from Invitrogen). Hindbrains and explants were examined under a fluorescent microscope (DMR6000, Leica) or a confocal microscope (FV1000, Olympus).

Cell culture, explant cuture, immunoprecipitation and Western blotting.

Please refer to the Extended Experimental Procedures.

Binding assay

HEK 293 cells (cell line from human embryonic kidney, Ad5 DNA transformed; ATCC) were transfected with various Slit-AP or Netrin1-AP plasmids using Lipofectamine 2000 reagent and grown for 48 hours. The supernatant was used directly without further

purification. AP activity was measured as previously described (He and Tessier-Lavigne, 1997) and the presence of the fusion protein in the supernatant at the expected molecular weight was confirmed by Western blot with anti-AP antibody (1:6000; GenHunter). Robo-AP, Slit-AP and Netrin1-AP binding on COS cells expressing Robos, DCC or Slit1-3 was performed as previously described (Renaud et al., 2008). Binding affinity was calculated as described in the Extended Experimental Procedures.

In utero electroporation

In utero electroporation of PN neurons was performed as described previously (Kawauchi et al., 2006), with some modifications described in the Extended Experimental Procedures.

Acknowledgements

This work was supported by grants from the Fondation pour la Recherche Médicale (Programme “équipe FRM”) and the Agence Nationale de la Recherche (ANR-08-MNP-030) to A.C. It was performed in the frame of the LABEX LIFESENSES (reference ANR-10-LABX-65) supported by French state funds managed by the ANR within the Investissements d'Avenir programme under reference ANR-11-IDEX-0004-02. P.Z was recipient of a post-doctoral fellowship from the Région ile de France (Neuropole). H.B is recipient of an ENP Graduate Program fellowship from the École des Neurosciences de Paris and the Région Ile-de-France (DIM Cerveau et Pensée). A.P. is a recipient of a fellowship under the program « Investissements d’Avenir » ANR-10-LABX-54 MEMO LIFE. Z.W was supported in part by a Bristol-Myers Squibb Postdoctoral Fellowship at the Rockefeller University. E.H. acknowledges funding by the Wellcome Trust.

References

Ackerman, S.L., and Knowles, B.B. (1998). Cloning and mapping of the UNC5C gene to human chromosome 4q21-q23. Genomics *52*, 205-208.

Alcantara, S., Ruiz, M., De Castro, F., Soriano, E., and Sotelo, C. (2000). Netrin 1 acts as an attractive or as a repulsive cue for distinct migrating neurons during the development of the cerebellar system. Development *127*, 1359-1372.

Altman, J., and Bayer, S.A. (1987). Development of the precerebellar nuclei in the rat: IV. The anterior precerebellar extramural migratory stream and the nucleus reticularis tegmenti pontis and the basal pontine gray. J Comp Neurol *257*, 529-552.

Amanchy, R., Periaswamy, B., Mathivanan, S., Reddy, R., Tattikota, S.G., and Pandey, A. (2007). A curated compendium of phosphorylation motifs. Nat Biotechnol *25*, 285-286.

Anastassiadis, T., Deacon, S.W., Devarajan, K., Ma, H., and Peterson, J.R. (2011). Comprehensive assay of kinase catalytic activity reveals features of kinase inhibitor selectivity. Nat Biotechnol *29*, 1039-1045.

Barton, R.A. (2012). Embodied cognitive evolution and the cerebellum. Philosophical transactions of the Royal Society of London Series B, Biological sciences *367*, 2097-2107.

Bashaw, G.J., Kidd, T., Murray, D., Pawson, T., and Goodman, C.S. (2000). Repulsive axon guidance: Abelson and Enabled play opposing roles downstream of the roundabout receptor. Cell *101*, 703-715.

Bloch-Gallego, E., Ezan, F., Tessier-Lavigne, M., and Sotelo, C. (1999). Floor plate and netrin-1 are involved in the migration and survival of inferior olivary neurons. J Neurosci *19*, 4407-4420.

Blom, N., Gammeltoft, S., and Brunak, S. (1999). Sequence and structure-based prediction of eukaryotic protein phosphorylation sites. Journal of molecular biology *294*, 1351-1362.

Brose, K., Bland, K.S., Wang, K.H., Arnott, D., Henzel, W., Goodman, C.S., Tessier-Lavigne, M., and Kidd, T. (1999). Slit proteins bind Robo receptors and have an evolutionarily conserved role in repulsive axon guidance. Cell *96*, 795-806.

Burgess, H.A., Johnson, S.L., and Granato, M. (2009). Unidirectional startle responses and disrupted left-right co-ordination of motor behaviors in robo3 mutant zebrafish. Genes Brain Behav *8*, 500-511.

Camurri, L., Mambetisaeva, E., Davies, D., Parnavelas, J., Sundaresan, V., and Andrews, W. (2005). Evidence for the existence of two Robo3 isoforms with divergent biochemical properties. Mol Cell Neurosci *30*, 485-493.

Canty, A.J., and Murphy, M. (2008). Molecular mechanisms of axon guidance in the developing corticospinal tract. Prog Neurobiol *85*, 214-235.

Chédotal, A. (2011). Further tales of the midline. Curr Opin Neurobiol *21*, 68-75.

Chen, Z., Gore, B.B., Long, H., Ma, L., and Tessier-Lavigne, M. (2008). Alternative splicing of the Robo3 axon guidance receptor governs the midline switch from attraction to repulsion. Neuron *58*, 325-332.

Choi, Y., Seeliger, M.A., Panjarian, S.B., Kim, H., Deng, X., Sim, T., Couch, B., Koleske, A.J., Smithgall, T.E., and Gray, N.S. (2009). N-myristoylated c-Abl tyrosine kinase localizes to the endoplasmic reticulum upon binding to an allosteric inhibitor. The Journal of biological chemistry *284*, 29005-29014.

Colak, D., Ji, S.J., Porse, B.T., and Jaffrey, S.R. (2013). Regulation of axon guidance by compartmentalized nonsense-mediated mRNA decay. Cell *153*, 1252-1265.

Di Meglio, T., Kratochwil, C.F., Vilain, N., Loche, A., Vitobello, A., Yonehara, K., Hrycaj, S.M., Roska, B., Peters, A.H., Eichmann, A.*, et al.* (2013). Ezh2 orchestrates topographic migration and connectivity of mouse precerebellar neurons. Science *339*, 204-207.

Di Meglio, T., Nguyen-Ba-Charvet, K.T., Tessier-Lavigne, M., Sotelo, C., and Chédotal, A.

(2008). Molecular mechanisms controlling midline crossing by precerebellar neurons. J Neurosci *28*, 6285-6294.

Dickson, B.J. (2002). Molecular mechanisms of axon guidance. Science *298*, 1959-1964.

Fan, X., Labrador, J.P., Hing, H., and Bashaw, G.J. (2003). Slit stimulation recruits Dock and Pak to the roundabout receptor and increases Rac activity to regulate axon repulsion at the CNS midline. Neuron *40*, 113-127.

Fazeli, A., Dickinson, S.L., Hermiston, M.L., Tighe, R.V., Steen, R.G., Small, C.G., Stoeckli, E.T., Keino-Masu, K., Masu, M., Rayburn, H.*, et al.* (1997). Phenotype of mice lacking functional Deleted in colorectal cancer (Dcc) gene. Nature *386*, 796-804.

Flicek, P., Amode, M.R., Barrell, D., Beal, K., Billis, K., Brent, S., Carvalho-Silva, D., Clapham, P., Coates, G., Fitzgerald, S.*, et al.* (2014). Ensembl 2014. Nucleic Acids Res *42*, D749-755.

Goodman, C.S. (1994). The likeness of being: phylogenetically conserved molecular mechanisms of growth cone guidance. Cell *78*, 353-356.

Goulding, M. (2009). Circuits controlling vertebrate locomotion: moving in a new direction. Nat Rev Neurosci *10*, 507-518.

Haeckel, E. (1866). Generelle moprhologie der organismen (Berlin, Georg Reimer).

Hao, J.C., Yu, T.W., Fujisawa, K., Culotti, J.G., Gengyo-Ando, K., Mitani, S., Moulder, G., Barstead, R., Tessier-Lavigne, M., and Bargmann, C.I. (2001). C. elegans slit acts in midline, dorsal-ventral, and anterior-posterior guidance via the SAX-3/Robo receptor. Neuron *32*, 25-38.

He, Z., and Tessier-Lavigne, M. (1997). Neuropilin is a receptor for the axonal chemorepellent Semaphorin III. Cell *90*, 739-751.

Heffner, C.D., Lumsden, A.G., and O'Leary, D.D. (1990). Target control of collateral extension and directional axon growth in the mammalian brain. Science *247*, 217-220.

Howitt, J.A., Clout, N.J., and Hohenester, E. (2004). Binding site for Robo receptors revealed by dissection of the leucine-rich repeat region of Slit. Embo J *23*, 4406-4412.

Jaworski, A., Long, H., and Tessier-Lavigne, M. (2010). Collaborative and specialized functions of Robo1 and Robo2 in spinal commissural axon guidance. J Neurosci *30*, 9445-9453.

Jen, J.C., Chan, W.M., Bosley, T.M., Wan, J., Carr, J.R., Rub, U., Shattuck, D., Salamon, G., Kudo, L.C., Ou, J.*, et al.* (2004). Mutations in a human ROBO gene disrupt hindbrain axon pathway crossing and morphogenesis. Science *304*, 1509-1513.

Jones, C.A., London, N.R., Chen, H., Park, K.W., Sauvaget, D., Stockton, R.A., Wythe, J.D., Suh, W., Larrieu-Lahargue, F., Mukouyama, Y.S.*, et al.* (2008). Robo4 stabilizes the vascular network by inhibiting pathologic angiogenesis and endothelial hyperpermeability. Nat Med *14*, 448-453.

Kawauchi, D., Taniguchi, H., Watanabe, H., Saito, T., and Murakami, F. (2006). Direct visualization of nucleogenesis by precerebellar neurons: involvement of ventricle-directed, radial fibre-associated migration. Development *133*, 1113-1123.

Keino-Masu, K., Masu, M., Hinck, L., Leonardo, E.D., Chan, S.S., Culotti, J.G., and Tessier-Lavigne, M. (1996). Deleted in Colorectal Cancer (DCC) encodes a netrin receptor. Cell *87*, 175-185.

Kennedy, T.E., Serafini, T., de la Torre, J.R., and Tessier-Lavigne, M. (1994). Netrins are diffusible chemotropic factors for commissural axons in the embryonic spinal cord. Cell *78*, 425-435.

Kidd, T., Bland, K.S., and Goodman, C.S. (1999). Slit is the midline repellent for the robo receptor in Drosophila. Cell *96*, 785-794.

Kidd, T., Brose, K., Mitchell, K.J., Fetter, R.D., Tessier-Lavigne, M., Goodman, C.S., and Tear, G. (1998). Roundabout controls axon crossing of the CNS midline and defines a

novel subfamily of evolutionarily conserved guidance receptors. Cell *92*, 205-215.

Kim, D., and Ackerman, S.L. (2011). The UNC5C netrin receptor regulates dorsal guidance of mouse hindbrain axons. J Neurosci *31*, 2167-2179.

Koch, A.W., Mathivet, T., Larrivee, B., Tong, R.K., Kowalski, J., Pibouin-Fragner, L., Bouvree, K., Stawicki, S., Nicholes, K., Rathore, N.*, et al.* (2011). Robo4 maintains vessel integrity and inhibits angiogenesis by interacting with UNC5B. Developmental cell *20*, 33-46.

Kolodziej, P.A., Timpe, L.C., Mitchell, K.J., Fried, S.R., Goodman, C.S., Jan, L.Y., and Jan, Y.N. (1996). frazzled encodes a Drosophila member of the DCC immunoglobulin subfamily and is required for CNS and motor axon guidance. Cell *87*, 197-204.

Korn, H., and Faber, D.S. (2005). The Mauthner cell half a century later: A neurobiological model for decision-making? Neuron *47*, 13-28.

Leonardo, E.D., Hinck, L., Masu, M., Keino-Masu, K., Ackerman, S.L., and Tessier-Lavigne, M. (1997). Vertebrate homologues of C. elegans UNC-5 are candidate netrin receptors. Nature *386*, 833-838.

Li, X., Meriane, M., Triki, I., Shekarabi, M., Kennedy, T.E., Larose, L., and Lamarche-Vane, N. (2002). The adaptor protein Nck-1 couples the netrin-1 receptor DCC (deleted in colorectal cancer) to the activation of the small GTPase Rac1 through an atypical mechanism. J Biol Chem *277*, 37788-37797.

Mambetisaeva, E.T., Andrews, W., Camurri, L., Annan, A., and Sundaresan, V. (2005). Robo family of proteins exhibit differential expression in mouse spinal cord and Robo-Slit interaction is required for midline crossing in vertebrate spinal cord. Dev Dyn *233*, 41-51.

Marillat, V., Sabatier, C., Failli, V., Matsunaga, E., Sotelo, C., Tessier-Lavigne, M., and Chédotal, A. (2004). The slit receptor Rig-1/Robo3 controls midline crossing by hindbrain precerebellar neurons and axons. Neuron *43*, 69-79.

Miyashita, T., Yeo, S.Y., Hirate, Y., Segawa, H., Wada, H., Little, M.H., Yamada, T., Takahashi, N., and Okamoto, H. (2004). PlexinA4 is necessary as a downstream target of Islet2 to mediate Slit signaling for promotion of sensory axon branching. Development *131*, 3705-3715.

Morlot, C., Thielens, N.M., Ravelli, R.B., Hemrika, W., Romijn, R.A., Gros, P., Cusack, S., and McCarthy, A.A. (2007). Structural insights into the Slit-Robo complex. Proc Natl Acad Sci U S A *104*, 14923-14928.

Nichols, D.H., and Bruce, L.L. (2006). Migratory routes and fates of cells transcribing the Wnt-1 gene in the murine hindbrain. Dev Dyn *235*, 285-300.

Notredame, C., Higgins, D.G., and Heringa, J. (2000). T-Coffee: A novel method for fast and accurate multiple sequence alignment. J Mol Biol *302*, 205-217.

O'Leary, D.D., and Terashima, T. (1988). Cortical axons branch to multiple subcortical targets by interstitial axon budding: implications for target recognition and "waiting periods". Neuron *1*, 901-910.

Phan, K.D., Croteau, L.P., Kam, J.W., Kania, A., Cloutier, J.F., and Butler, S.J. (2011). Neogenin may functionally substitute for Dcc in chicken. PLoS One *6*, e22072.

Philipp, M., Niederkofler, V., Debrunner, M., Alther, T., Kunz, B., and Stoeckli, E.T. (2012). RabGDI controls axonal midline crossing by regulating Robo1 surface expression. Neur Dev *7*, 36.

Rajagopalan, S., Nicolas, E., Vivancos, V., Berger, J., and Dickson, B.J. (2000). Crossing the midline: roles and regulation of Robo receptors. Neuron *28*, 767-777.

Renaud, J., Kerjan, G., Sumita, I., Zagar, Y., Georget, V., Kim, D., Fouquet, C., Suda, K., Sanbo, M., Suto, F.*, et al.* (2008). Plexin-A2 and its ligand, Sema6A, control nucleus-centrosome coupling in migrating granule cells. Nat Neurosci *11*, 440-449.

Renier, N., Schonewille, M., Giraudet, F., Badura, A., Tessier-Lavigne, M., Avan, P., De

Zeeuw, C.I., and Chédotal, A. (2010). Genetic dissection of the function of hindbrain axonal commissures. PLoS Biol *8*, e1000325.

Richards, L.J., Plachez, C., and Ren, T. (2004). Mechanisms regulating the development of the corpus callosum and its agenesis in mouse and human. Clin Genet *66*, 276-289.

Rodriguez, C.I., and Dymecki, S.M. (2000). Origin of the precerebellar system. Neuron *27*, 475-486.

Sabatier, C., Plump, A.S., Le, M., Brose, K., Tamada, A., Murakami, F., Lee, E.Y., and Tessier-Lavigne, M. (2004). The divergent Robo family protein rig-1/Robo3 is a negative regulator of slit responsiveness required for midline crossing by commissural axons. Cell *117*, 157-169.

Sandilands, E., Cans, C., Fincham, V.J., Brunton, V.G., Mellor, H., Prendergast, G.C., Norman, J.C., Superti-Furga, G., and Frame, M.C. (2004). RhoB and actin polymerization coordinate Src activation with endosome-mediated delivery to the membrane. Dev Cell *7*, 855-869.

Sarro, J., Andrews, E., Sun, L., Behura, S.K., Tan, J.C., Zeng, E., Severson, D.W., and Duman-Scheel, M. (2013). Requirement for commissureless2 function during dipteran insect nerve cord development. Dev Dyn *242*, 1466-1477.

Schweitzer, J., Lohr, H., Bonkowsky, J.L., Hubscher, K., and Driever, W. (2013). Sim1a and Arnt2 contribute to hypothalamo-spinal axon guidance by regulating Robo2 activity via a Robo3-dependent mechanism. Development *140*, 93-106.

Serafini, T., Colamarino, S.A., Leonardo, E.D., Wang, H., Beddington, R., Skarnes, W.C., and Tessier-Lavigne, M. (1996). Netrin-1 is required for commissural axon guidance in the developing vertebrate nervous system. Cell *87*, 1001-1014.

Shim, S., Kwan, K.Y., Li, M., Lefebvre, V., and Sestan, N. (2012). Cis-regulatory control of corticospinal system development and evolution. Nature *486*, 74-79.

Simpson, J.H., Kidd, T., Bland, K.S., and Goodman, C.S. (2000). Short-range and long-range guidance by slit and its Robo receptors. Robo and Robo2 play distinct roles in midline guidance. Neuron *28*, 753-766.

Spitzweck, B., Brankatschk, M., and Dickson, B.J. (2010). Distinct protein domains and expression patterns confer divergent axon guidance functions for Drosophila Robo receptors. Cell *140*, 409-420.

Stein, E., and Tessier-Lavigne, M. (2001). Hierarchical organization of guidance receptors: silencing of netrin attraction by slit through a Robo/DCC receptor complex. Science *291*, 1928-1938.

Suarez, R., Gobius, I., and Richards, L.J. (2014). Evolution and development of interhemispheric connections in the vertebrate forebrain. Front Hum Neurosci *8*, 497.

Twamley-Stein, G.M., Pepperkok, R., Ansorge, W., and Courtneidge, S.A. (1993). The Src family tyrosine kinases are required for platelet-derived growth factor-mediated signal transduction in NIH 3T3 cells. Proc Natl Acad Sci U S A *90*, 7696-7700.

Vilella, A.J., Severin, J., Ureta-Vidal, A., Heng, L., Durbin, R., and Birney, E. (2009). EnsemblCompara GeneTrees: Complete, duplication-aware phylogenetic trees in vertebrates. Gen Res *19*, 327-335.

Wullimann, M.F., Mueller, T., Distel, M., Babaryka, A., Grothe, B., and Koster, R.W. (2011). The long adventurous journey of rhombic lip cells in jawed vertebrates: a comparative developmental analysis. Front Neuroanat *5*, 27.

Xu, K., Wu, Z., Renier, N., Antipenko, A., Tzvetkova-Robev, D., Xu, Y., Minchenko, M., Nardi-Dei, V., Rajashankar, K.R., Himanen, J.*, et al.* (2014). Neural migration. Structures of netrin-1 bound to two receptors provide insight into its axon guidance mechanism. Science *344*, 1275-1279.

Yang, Z. (2007). PAML 4: phylogenetic analysis by maximum likelihood. Mol Biol Evol *24*,

1586-1591.

Yee, K.T., Simon, H.H., Tessier-Lavigne, M., and O'Leary, D.M. (1999). Extension of long leading processes and neuronal migration in the mammalian brain directed by the chemoattractant netrin-1. Neuron *24*, 607-622.

Yuan, S.S., Cox, L.A., Dasika, G.K., and Lee, E.Y. (1999). Cloning and functional studies of a novel gene aberrantly expressed in RB-deficient embryos. Dev Biol *207*, 62-75.

Figure legends

Figure 1.

Evolution of the *Robo* gene family and mammalian specific structure of Robo3

(A) The phylogenetic reconstruction of the evolution of the *Robo1*, *Robo2* and *Robo3* genes shows that *Robo2* and *Robo3* are evolutionarily closer to each other than either is to *Robo1*. The scale represents the rate of substitution per base pair. (B) Plausible scenarios of Robo evolution, in which tandem duplicates were duplicated during two rounds (1R and 2R) of WGD. (C) Domain architecture of Robo3 containing 5 immunoglobulin (Ig) and 3 fibronectin type III (FN) domains, and 3 conserved domains (CC) in the intracellular part (Sabatier et al., 2004; Yuan et al., 1999). Identity percentage of vertebrates Robo1, Robo2 and Robo3 Ig1 domains shows high conservation of these sequences except in mammalian Robo3 sequences. (D) Analysis of positive selection in the Robo Ig1 protein sequences. The LRT test comparing the null model (neutrality) to the alternative model (positive selection) over the entire Robo3 coding sequence is significant (df=1, $2*\Delta lnL = 9.552$, Pval=0.0025). In the Ig1 domain, Robo3 shows 14 sites under positive selection in the stem branch of mammals (red) and 4 sites in the stem branch of amniotes. No other internal branch show sites under positive selection (BEB > 0.5). (E) Location of Asn88, Lys90 and Leu130 in the crystallized Slit2-D2-Robo1 Ig1 complex

(Morlot et al., 2007). Slit2-D2 is shown as a blue surface with four key Robo binding residues (Howitt et al., 2004) highlighted in green. The interacting face of Robo1 Ig1 is shown as a cartoon with selected side chains in atomic detail. (F) Alignment of the first Ig domains of mammalian and non-mammalian Robo3 and human Robo1 and Robo2. Ten residues that are involved in Slit2 binding to Robo1 according to the crystal structure of Morlot et al. (2007) are indicated by asterisks. Red asterisks indicate the two substitutions that are not conservative, in the Slit-binding domain and detected under positive selection. Mammalian specific residues are represented in blue, corresponding amino acids conserved in non-mammalians and other Robos are represented in red. Sequence numbers are indicated at the top for human Robo3 protein and at the bottom for human Robo1. See also Figure S1.

Figure 2

Mammalian Robo3 does not bind Slits with high affinity

(A) hSlit2-D2-AP binds to COS cells expressing mammalian rRobo1A and rRobo2B but not to cells expressing mammalian Robo3A.1 or Robo3B.2. (B) Slit binding is lost in cells expressing rRobo1$^{N88P/K90R/L130P}$ or rRobo1^{L130P} but restored in cells expressing mRobo3$^{P84N/R86K/P126L}$ or mRobo3^{P126L}. (C) zSlit2-D2-AP binds to COS cells expressing zRobo2 or zRobo3A.1 but not to cells expressing zRobo3$^{N83P/K85R/L125P}$ or zRobo3^{L125P}**.** (D) xSlit2-D2-AP binds to COS cells expressing xRobo3A.1 but not xRobo3$^{N85P/K87R/L127P}$. (E) Scatchard analysis of Slit2 binding affinity to Robo receptors. The data shown are representative of at least 3 independent experiments. See also Figure S2.

Figure 3

Differential tyrosine phosphorylation responses of mammalian and non-mammalian Robo3 to Slit and Netrin.

(A, B) COS-7 cells expressing various Robo3 constructs were stimulated with 250ng/ml Slit2 for 10 min and phosphorylation changes analyzed by Western blotting. (A) Slit2 induces dephosphorylation of zRobo3 (58.65% ± 10.59 of control, n=5, p= 0.0075, **), but does not affect phosphorylation of mRobo3 (103.04% ± 6.24 of control, n=3, ns). (B) By contrast, the phosphorylation of mutated zRobo3 (zRobo3^{3xmut} , i.e. zRobo3$^{N85P/K87R/L125P}$) which do not bind Slit2 (see also Figure 2) is not modified by Slit2 whereas mutated mouse Robo3 (mRobo3^{3xmut}, i.e. mRobo3$^{P84N/R86K/P126L}$) behaves like non-mammalian Robo3 and are dephosphorylated by Slit2 (56.55% ± 13.51 of control, n=8, p= 0.0015, **). (C) Netrin-1 increases phosphorylation of mRobo3 (447.79% ± 17.81 of control, n=10 experiments, p< 0.0001, ****), but has no effect on zRobo3 (78.93% ± 25.62 of control, n=3, ns). Histograms represent quantification of phospho-signals normalized to total Robo3 amounts, Mann-Whitney U test. (D) Netrin-1 stimulation of COS-7 cells expressing wild type (wt) or mRobo3 mutated at either position 1002 (Y1002F) or 1019 (Y1019F) shows mRobo3 is selectively phosphorylated on Y1019, since a phospho-dead mutant at this position lacks a phosphorylation response (Y1002F: 126.61% ± 16.55 of control; Y1019F: 29.54% ± 5.85% of control, n=6, repeated measures one-way ANOVA with Bonferroni corrected comparison for selected pairs of means without correction for multiple comparisons, error bar SEM ; asterisks indicate p value range, where p < 0.05 = *, p < 0.01 = **, p < 0.001 = ***, p < 0.0001 = ****). (E) The Src-kinase inhibitor PP2 leads to complete inhibition of phosphorylation on endogenous Robo3 in mouse P19 cells. Phosphorylation response was quantified by immunoblotting and densitometric analysis (+Netrin-1: 344.69% ± 165.77 of control; +Netrin-1 +PP2: 4.06% ± 2.08 of control, n=4, repeated measures one-way ANOVA with Bonferroni corrected comparison for selected

pairs of means without correction for multiple comparisons, error bar SEM; asterisks indicate p value range, where $p < 0.05$ = *, $p < 0.01$ = **, $p < 0.001$ = ***, $p < 0.0001$ = ****). (F) The phosphorylation of mRobo3 was compared by phospho-tyrosine specific immunoblots of COS-7 cells co-expressing mRobo3 and wild type (wt) or dominant-negative (K295M) c-Src constructs and phospho-signal was quantified (3.07% ± 1.19 of control, n=5 experiments, P=0.0075, **, error bar SEM). (G) Alignment of the CC0 domain of Robo receptors from various species illustrating the conservation of the Y1019 residue across evolution. (H) Model of differential activation of Robo3 in mammalian and non-mammalian species. See also Figure S3.

Figure 4. DCC and Robo3 form a molecular complex

(A) Co-immunoprecipitation of endogenous Robo3 and DCC in E14.5 hindbrain extracts. DCC/Robo3 interaction is detected in *DCC*$^{+/+}$ controls and *DCC*$^{+/-}$ heterozygous embryos but is lost in *DCC*$^{-/-}$ mutant and *Robo3*$^{-/-}$ mutant. DCC and Robo3 still interact in *Netrin-1* mutant (*Ntr1*$^{-/-}$). (B) mRobo3A.1-myc (Robo3) co-immunoprecipitates with hDCC-HA in HEK293 cells independently of Netrin-1. (C) Robo3A.1 does not co-immunoprecipitate with DCC-V5 deleted of the P3 domain (DCC∆P3-V5). (D) Robo3A.1 lacking the CC2 and CC3 domains fails to bind to DCC. See also Figure S4.

Figure 5

Ventral migration defects of pontine neurons in *Robo3, DCC* and *Netrin-1* knockouts.

(A, B) Migration pathway of PN neurons (a, anterior; p, posterior) in wild type embryos after whole-mount *in situ* hybridization for *Barlh1* (A; E16.5) or *in utero* electroporation of a GFP plasmid (B; E15.5). In a first phase (1 in B), PN neurons leave the rhombic lip (RL)

and migrate anteriorly to the root of the trigeminal nerve (Vr). During phase 2, they migrate ventrally towards the floor plate (midline indicated by a dotted line on all panels). (C) Schematic of pontine neuron migratory stream. Pontine neurons leave the rhombic lip dorsally (d) and migrate towards the floor plate (FP). They turn ventrally (v) upon reaching the Vr. (D) Migration pathway of PN neurons in E16.5 *Robo3*$^{-/-}$ embryos after whole-mount *in situ* hybridization for *Barhl1* (D) or *in utero* electroporation of a GFP plasmid (E). In a first phase (1 in E) PN neurons migrate normally to the Vr. They next turn ventrally (2) but then reorient dorsally (3) and never contact the ventral midline. (F) An overlay image of wild type (electroporated with a GFP plasmid) and *Robo3*$^{-/-}$ (electroporated with a RFP plasmid) embryos, illustrating the position of the abnormal dorsal turning point (arrow). (G) E16.5 *Netrin1*$^{-/-}$ embryos electroporated at E13.5 with GFP. PN neurons migrate to Vr and turn ventrally, before reorienting dorsally as in *Robo3*$^{-/-}$ embryos. (H) E16.5 *DCC*$^{-/-}$ embryos electroporated at E13.5 with GFP. Some PN neurons leave the main stream dorsally and ventrally before reaching the Vr. Many PN neurons turn ventrally but then reorient dorsally (arrowheads).(I) DCC is still highly expressed in PN migration stream (arrowhead) of *Robo3*$^{-/-}$ mutant.(J-L) Cell surface biotinylation of Robo3 and DCC receptor protein expression in E14.5 hindbrain tissue. In *Robo3* KO (J, K), the expression of DCC is similar to wild type and heteorozygous embryos and likewise Robo3 expression is unchanged in *DCC* knockout (L, K).

Abbreviations, Cer,cerebellum. Scale bars: 400 μm in A, D, F; 200 μm in B; 360 μm in E; 250 μm in G, H; 500 in I.

Figure 6.

Netrin-1-attraction of PN neurons is abrogated in *Robo3* KO.

(A-E) E14.5 rhombic lip (rl) explants from wild type or *Robo3*$^{-/-}$ embryos cultured for 48-72 hr in collagen gels next to floor plate explants (fp) or Netrin-1 expressing cell aggregates (asterisk in C and E). (A) In wild type, streams of GFP+ PN neurons (arrowheads) migrate out of the explants towards floor plate, whereas in explants from *Robo3*$^{-/-}$ embryos (B) GFP+ neurons (arrowheads) fail to leave the explant. (C-E) Wild type PN neurons (labelled by Pax6 and ßIII-tubulin) are attracted by aggregates of Netrin-1 expressing cells (C, D), whereas PN neurons from *Robo3* KO are not (E). D is a higher magnification of the area indicated by an arrow in C. (F, G) The number of neuron bundles (see arrowheads in A, D and methods) were counted for each explant (n is the number of explants). Quantifications of neuron bundles per explant (mean value with SEM; **p<0.005) and percentages of explants with (response) and without (no response) neuron bundles are shown. (H) Mouse E11.5 dorsal spinal cord explants from wild type (WT), or *Robo3* mutant, were cultured with different concentrations of Netrin-1. Axon outgrowth was visualized and quantified by immunohistochemistry (IHC) for ßIII-tubulin. Compared to wild type explants, *Robo3* mutant explants showed less Netrin-1 induced outgrowth. (n=3; plot for mean and s.e.m.; two-tailed unpaired t test: *p<0.05 and **p<0.005.). Scale bars: 250 µm in A, B; 130 µm in C, E; 80 µm in D. See also Movie S1.

Figure 7

Rescue of *Robo3*$^{-/-}$ pontine neuron midline migration by mammalian but not non-mammalian Robo3.

(A, B) Rescue experiments by *in utero* electroporations of PN neurons in *Wnt1::cre;Robo3*$^{lox/lox}$ hindbrains co-electroporated at E13.5 with mouse Robo3A.1 and GFP, stained for PN marker Barhl1. Note that on the non electroporated side, Barhl1+ PN neurons do not migrate ventrally. By contrast electroporated PN neurons and their axons

reach the floor plate (dotted line) and/or cross it. (B) illustrates a higher magnification of the area near the floor plate. (C) E17.5 *Robo3*$^{-/-}$ hindbrain co-electroporated at E13.5 with zebrafish Robo3A.1 and GFP. None of the electroporated pontine neurons or their axons leave the abberant migratory stream and/or reach the midline (dotted line). (D) illustrates a higher magnification of the area near the floor plate. (E-H) Dorsal views of confocal z-projections of the hindbrain of 72 hpf zebrafish embryos labelled with 3A10 antibody. Anterior is towards the left. Normal midline crossing of MA axons in control (E), *hsp70l:zrobo3a.1*^{L125P} (G) and *hsp70l:zrobo3a.1*^{N83PK85RL125P} (H) embryos. In *hsp70l:zrobo3.1* embryos extra midline crossing events of MA axons are shown. (F). The arrows in E-H indicate normal midline crossing of MA axons, the arrowhead in F points to an extra MA axon midline crossing event.

Scale bars: 250μm in A; 50μm in B and E; 300μm in C; 150μm in D.

See also Figures S6 and S7.

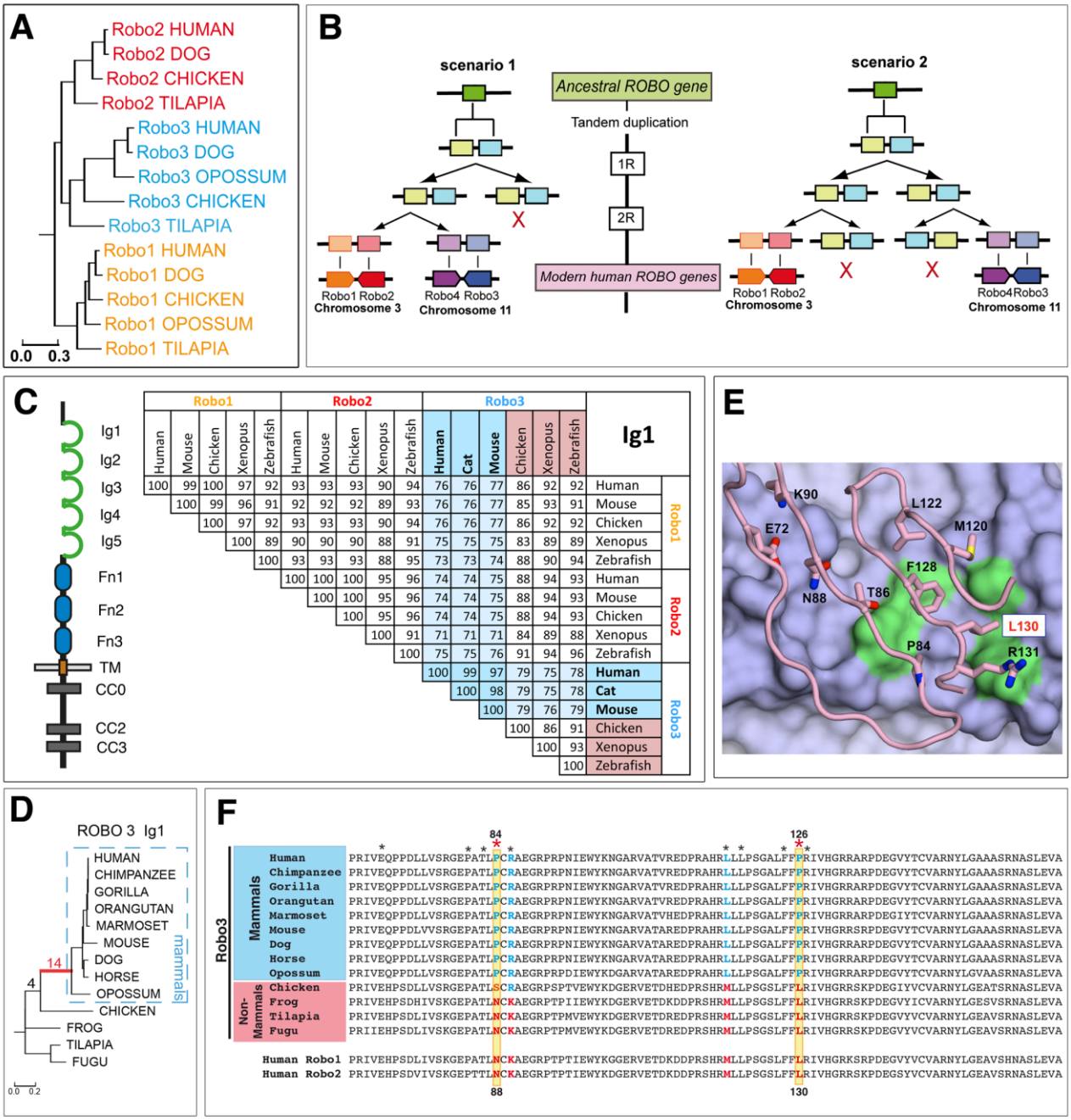
A
Robo2 HUMAN
Robo2 DOG
Robo2 CHICKEN
Robo2 TILAPIA
Robo3 HUMAN
Robo3 DOG
Robo3 OPOSSUM
Robo3 CHICKEN
Robo3 TILAPIA
Robo1 HUMAN
Robo1 DOG
Robo1 CHICKEN
Robo1 OPOSSUM
Robo1 TILAPIA
0.0 0.3
B
scenario 1
Ancestral ROBO gene
Tandem duplication
1R
2R
Modern human ROBO genes
Robo1 Robo2
Chromosome 3
Robo4 Robo3
Chromosome 11
scenario 2
C
Ig1
Ig2
Ig3
Ig4
Ig5
Fn1
Fn2
Fn3
TM
CC0
CC2
CC3
Robo1
Robo2
Robo3
Ig1
Human Mouse Chicken Xenopus Zebrafish
Human Cat Mouse Chicken Xenopus Zebrafish
E
K90
L122
E72
M120
F128
N88
T86
L130
P84
R131
D
ROBO 3 Ig1
HUMAN
CHIMPANZEE
GORILLA
ORANGUTAN
MARMOSET
MOUSE
DOG
HORSE
OPOSSUM
CHICKEN
FROG
TILAPIA
FUGU
mammals
14
4
0.0 0.2
F
Robo3
Mammals
Non-Mammals
Human
Chimpanzee
Gorilla
Orangutan
Marmoset
Mouse
Dog
Horse
Opossum
Chicken
Frog
Tilapia
Fugu
Human Robo1
Human Robo2
84
88
126
130

Figure 1

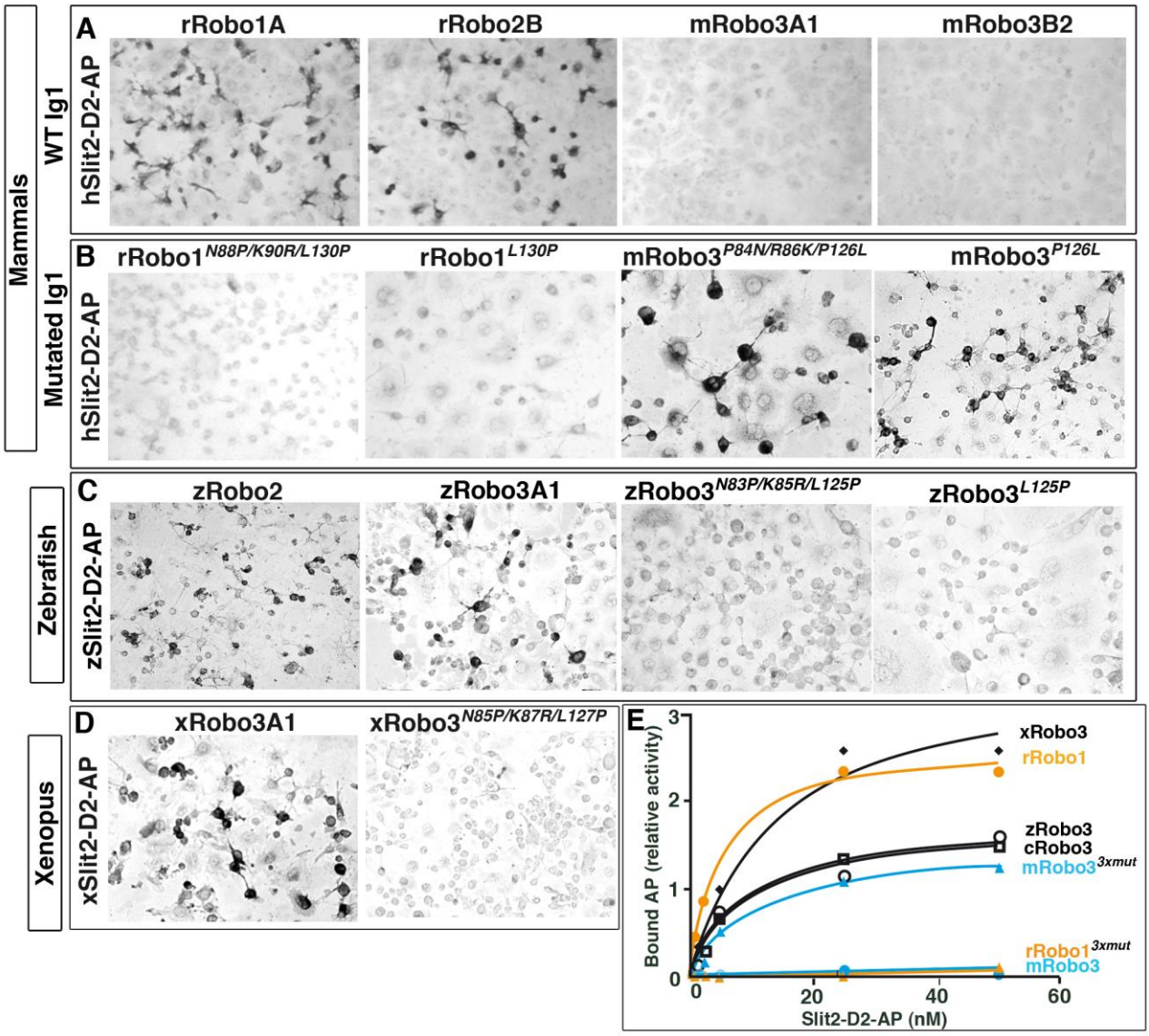
Mammals
WT Ig1
Mutated Ig1
A
rRobo1A
rRobo2B
mRobo3A1
mRobo3B2
hSlit2-D2-AP
B
rRobo1N88P/K90R/L130P
rRobo1L130P
mRobo3P84N/R86K/P126L
mRobo3P126L
hSlit2-D2-AP
Zebrafish
C
zRobo2
zRobo3A1
zRobo3N83P/K85R/L125P
zRobo3L125P
zSlit2-D2-AP
Xenopus
D
xRobo3A1
xRobo3N85P/K87R/L127P
xSlit2-D2-AP
E
Bound AP (relative activity)
Slit2-D2-AP (nM)
xRobo3
rRobo1
zRobo3
cRobo3
mRobo33xmut
rRobo13xmut
mRobo3
0
1
2
3
0
20
40
60

Figure 2

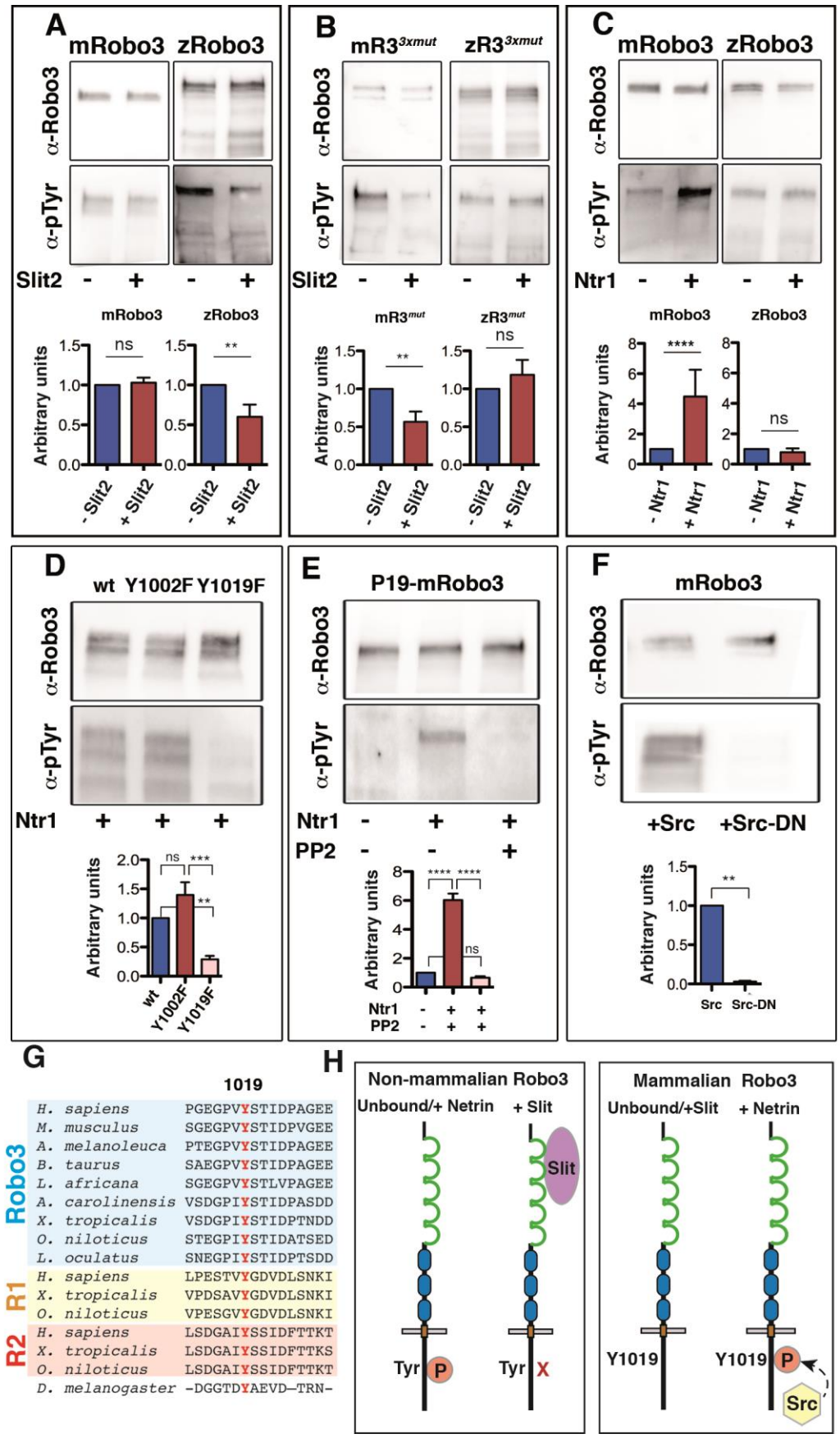
A
mRobo3 zRobo3
α-Robo3
α-pTyr
Slit2 - + - +
mRobo3 zRobo3
Arbitrary units
ns
**
- Slit2
+ Slit2
B
mR3 3xmut zR3 3xmut
α-Robo3
α-pTyr
Slit2 - + - +
mR3 mut zR3 mut
**
ns
- Slit2
+ Slit2
C
mRobo3 zRobo3
α-Robo3
α-pTyr
Ntr1 - + - +
mRobo3 zRobo3
****
ns
- Ntr1
+ Ntr1
D
wt Y1002F Y1019F
α-Robo3
α-pTyr
Ntr1 + + +
ns ***
**
wt
Y1002F
Y1019F
E
P19-mRobo3
α-Robo3
α-pTyr
Ntr1 - + +
PP2 - - +
**** ****
ns
F
mRobo3
α-Robo3
α-pTyr
+Src +Src-DN
**
Src
Src-DN
G
1019
H. sapiens PGEGPVYSTIDPAGEE
M. musculus SGEGPVYSTIDPVGEE
A. melanoleuca PTEGPVYSTIDPAGEE
B. taurus SAEGPVYSTIDPAGEE
L. africana SGEGPVYSTLVPAGEE
A. carolinensis VSDGPIYSTIDPASDD
X. tropicalis VSDGPIYSTIDPTNDD
O. niloticus STEGPIYSTIDATSED
L. oculatus SNEGPIYSTIDPTSDD
Robo3
H. sapiens LPESTVYGDVDLSNKI
X. tropicalis VPDSAVYGDVDLSNKI
O. niloticus VPESGVYGDVDLSNKI
R1
H. sapiens LSDGAIYSSIDFTTKT
X. tropicalis LSDGAIYSSIDFTTKS
O. niloticus LSDGAIYSSIDFTTKT
R2
D. melanogaster -DGGTDYAEVD-TRN-
H
Non-mammalian Robo3
Unbound/+ Netrin
+ Slit
Slit
Tyr P
Tyr X
Mammalian Robo3
Unbound/+Slit
+ Netrin
Y1019
Y1019 P
Src

Figure 3

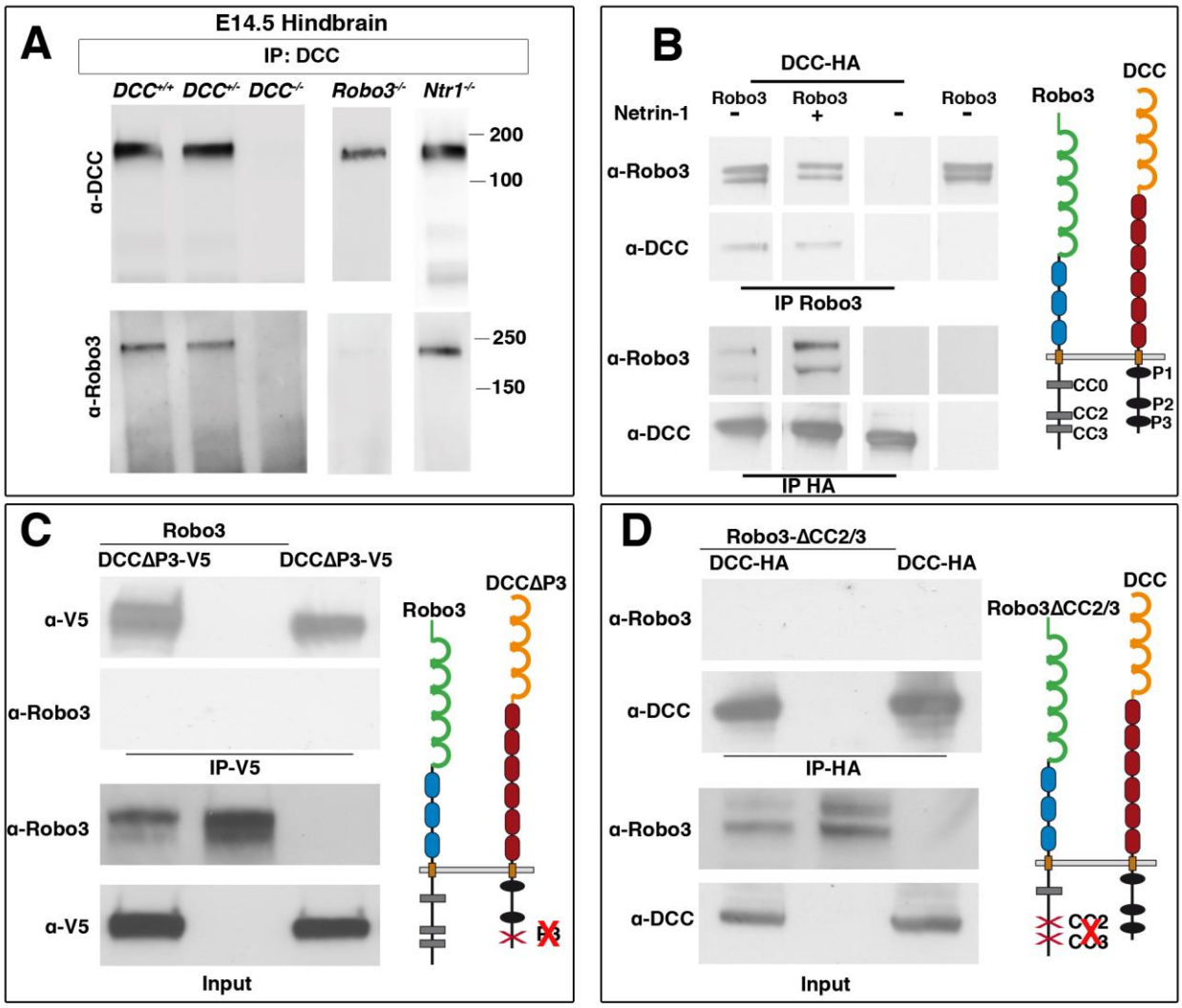
A
E14.5 Hindbrain
IP: DCC
DCC+/+ DCC+/- DCC-/- Robo3-/- Ntr1-/-
α-DCC
α-Robo3
200
100
250
150
B
DCC-HA
Netrin-1
Robo3 - Robo3 + - Robo3 -
α-Robo3
α-DCC
IP Robo3
α-Robo3
α-DCC
IP HA
Robo3
DCC
CC0
CC2
CC3
P1
P2
P3
C
Robo3
DCCΔP3-V5 DCCΔP3-V5
α-V5
α-Robo3
IP-V5
α-Robo3
α-V5
Input
DCCΔP3
Robo3
D
Robo3-ΔCC2/3
DCC-HA DCC-HA
α-Robo3
α-DCC
IP-HA
α-Robo3
α-DCC
Input
DCC
Robo3ΔCC2/3
CC2
CC3

Figure 4

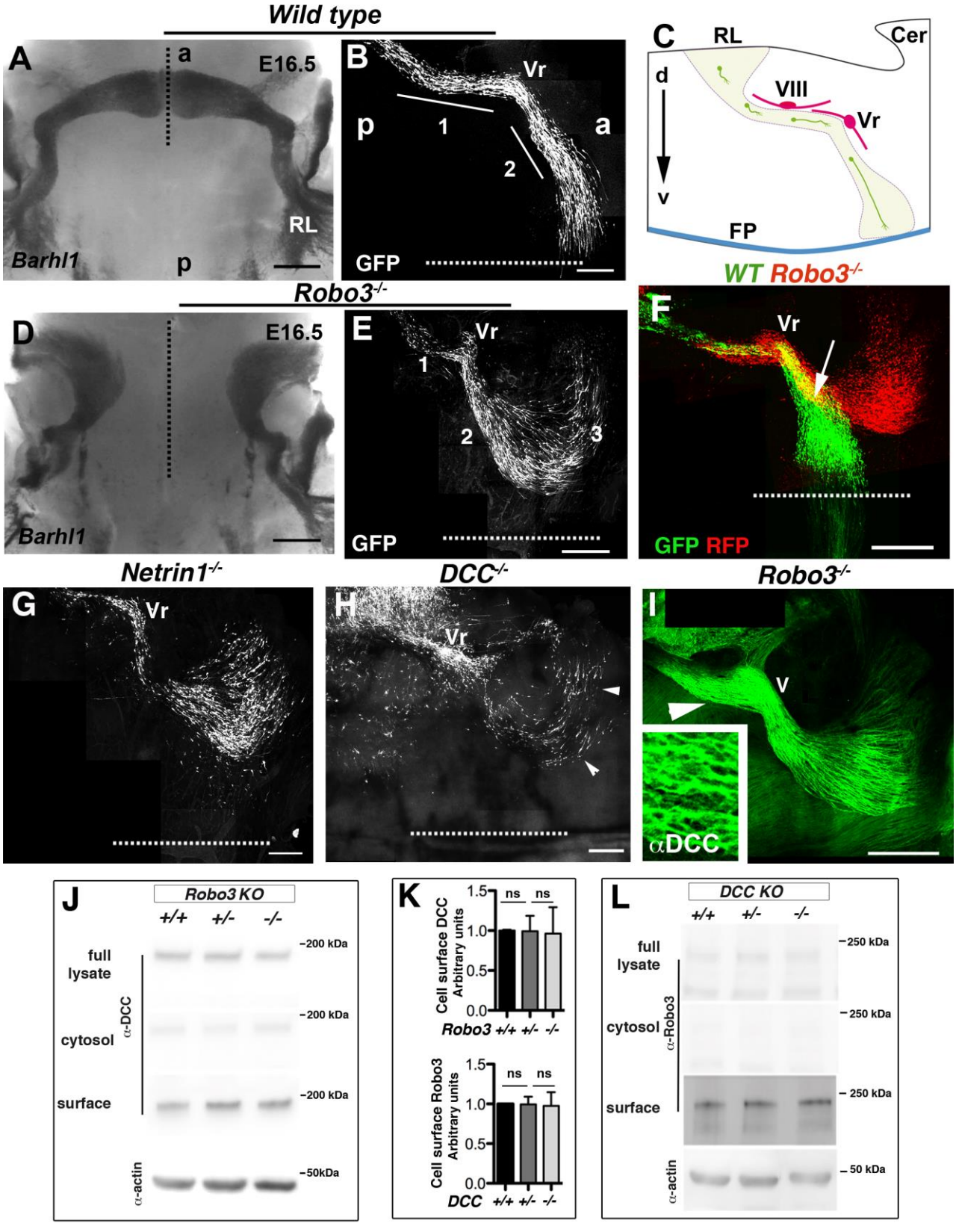
Wild type
A
a
E16.5
RL
Barhl1
p
B
Vr
p
1
a
2
GFP
C
RL
Cer
d
VIII
Vr
v
FP
WT Robo3-/-
Robo3-/-
D
E16.5
Barhl1
E
Vr
1
2
3
GFP
F
Vr
GFP RFP
Netrin1-/-
DCC-/-
Robo3-/-
G
Vr
H
Vr
I
V
αDCC
J
Robo3 KO
+/+ +/- -/-
full lysate
cytosol
surface
α-DCC
α-actin
200 kDa
200 kDa
200 kDa
50kDa
K
Cell surface DCC Arbitrary units
1.5
1.0
0.5
0.0
ns ns
Robo3 +/+ +/- -/-
Cell surface Robo3 Arbitrary units
1.5
1.0
0.5
0.0
ns ns
DCC +/+ +/- -/-
L
DCC KO
+/+ +/- -/-
full lysate
cytosol
surface
α-Robo3
α-actin
250 kDa
250 kDa
250 kDa
50 kDa

Figure 5

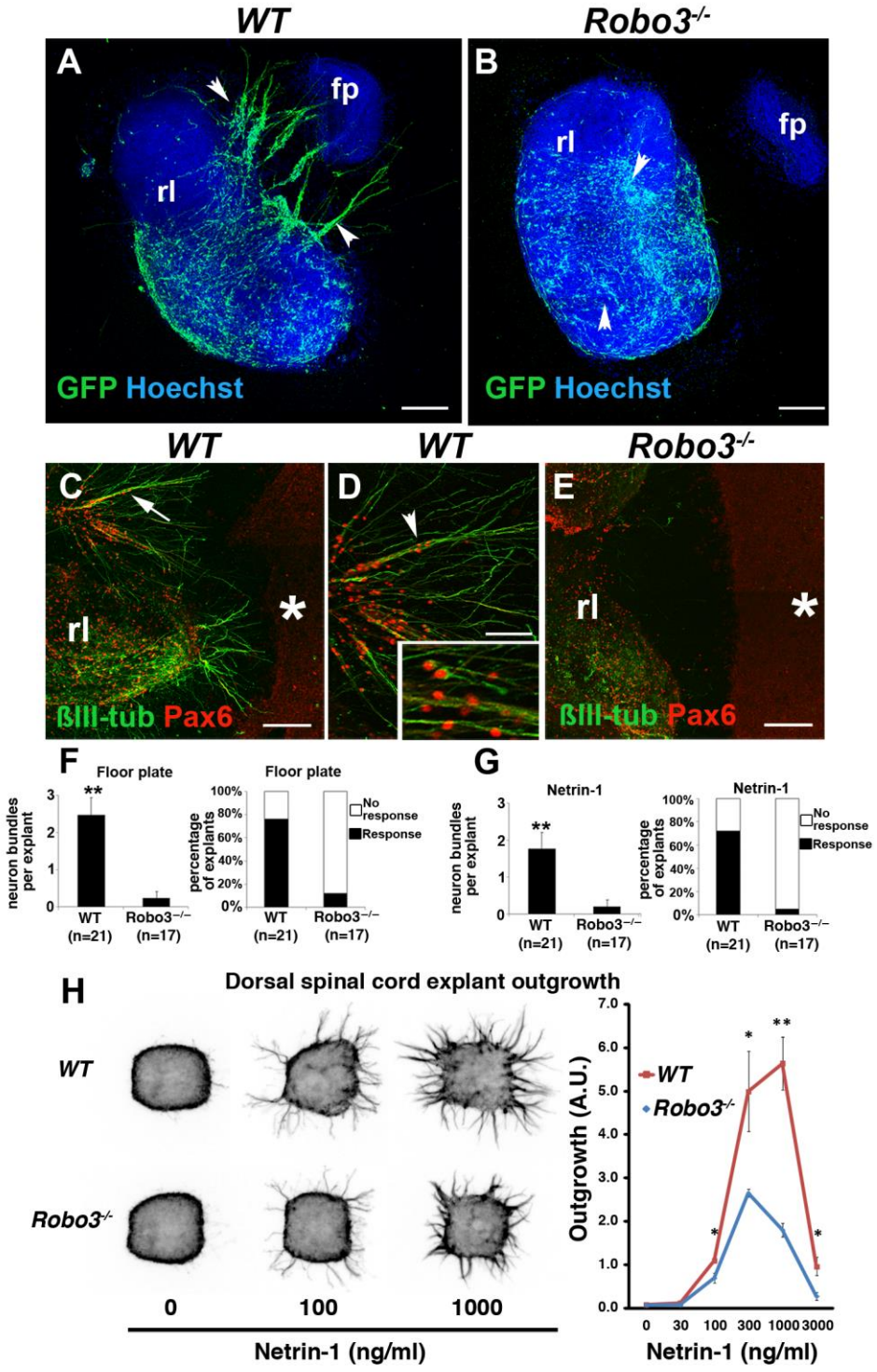
WT
Robo3-/-
A
fp
rl
GFP Hoechst
B
rl
fp
GFP Hoechst
WT
WT
Robo3-/-
C
rl
*
ßIII-tub Pax6
D
E
rl
*
ßIII-tub Pax6
F
Floor plate
neuron bundles per explant
**
WT (n=21)
Robo3−/− (n=17)
Floor plate
percentage of explants
No response
Response
G
Netrin-1
neuron bundles per explant
Netrin-1
percentage of explants
No response
Response
H
Dorsal spinal cord explant outgrowth
WT
Robo3-/-
0
100
1000
Netrin-1 (ng/ml)
Outgrowth (A.U.)
WT
Robo3-/-
0 30 100 300 1000 3000
Netrin-1 (ng/ml)

Figure 6

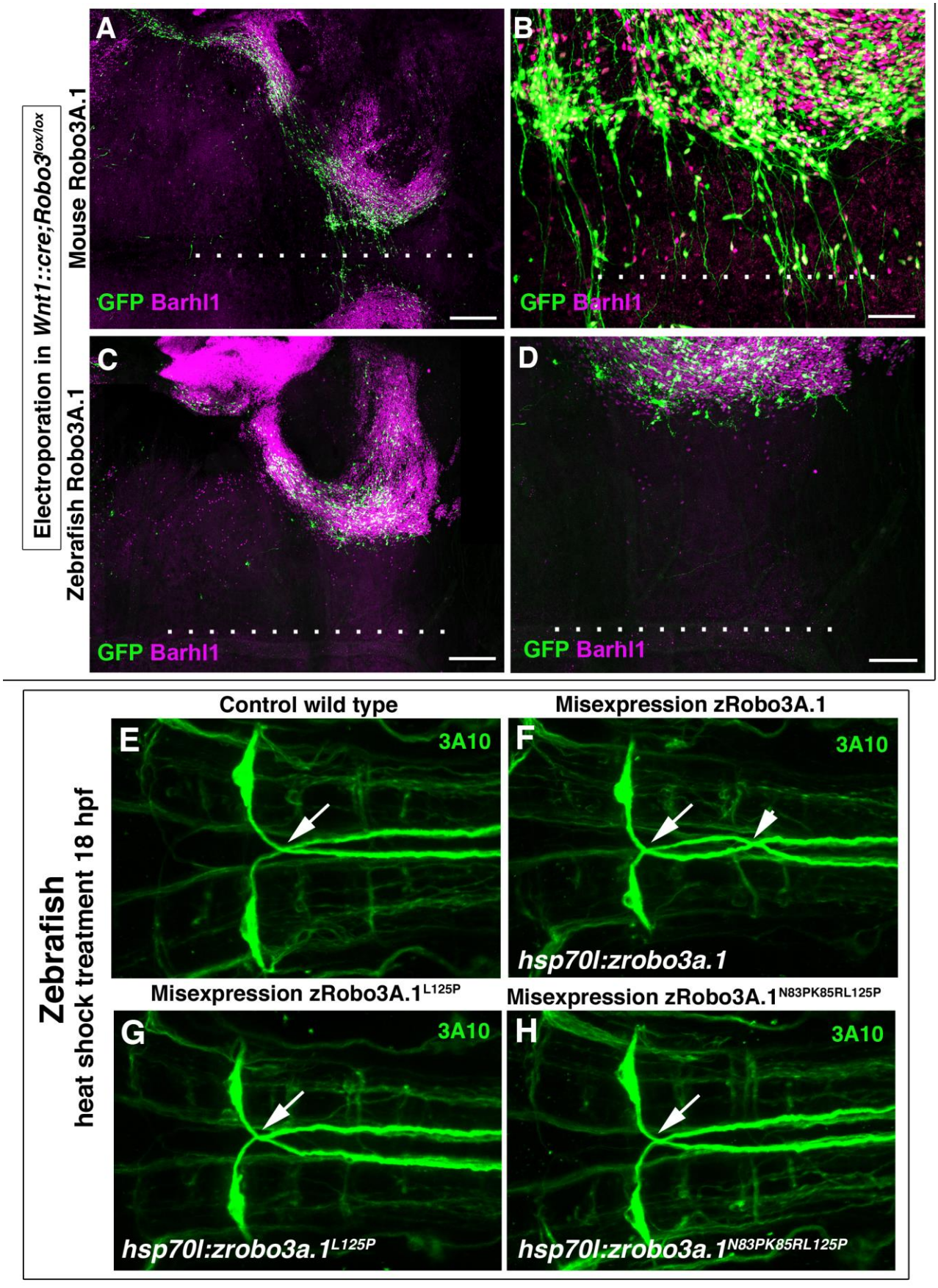
Electroporation in Wnt1::cre;Robo3lox/lox
Mouse Robo3A.1
Zebrafish Robo3A.1
A
GFP Barhl1
B
GFP Barhl1
C
GFP Barhl1
D
GFP Barhl1
Zebrafish
heat shock treatment 18 hpf
Control wild type
E
3A10
Misexpression zRobo3A.1
F
3A10
hsp70l:zrobo3a.1
Misexpression zRobo3A.1L125P
G
3A10
hsp70l:zrobo3a.1L125P
Misexpression zRobo3A.1N83PK85RL125P
H
3A10
hsp70l:zrobo3a.1N83PK85RL125P

Figure 7

Contents of Supplementary Material for:

Signaling Switch of the Axon Guidance Receptor Robo3 during Vertebrate Evolution.

Pavol Zelina, Heike Blockus, Yvrick Zagar, Amélie Péres, François Friocourt, Zhuaho Wu, Nicolas Rama, Coralie Fouquet, Erhard Hohenester, Marc Tessier-Lavigne, Jörn Schweitzer, Hugues Roest Crollius and Alain Chédotal

Extended experimental procedures

Expression plasmids.

The following plasmids were used: full-length myc-tagged mouse Robo3A.1 (Robo3A.1-myc; Chen et al., 2008), full-length myc-tagged mouse Robo3B.2 (Robo3B.2-myc; Sabatier et al., 2004), full length human Robo3A.1 (Origene clone RC216411), full-length myc-tagged rat Robo1, full-length rat Robo2 (Kidd et al., 1998), full-length human DCC (Mille et al., 2009) and full-length zebrafish Robo3A.1 (*pMErobo3a.*1; Schweitzer et al., 2013). Full-length human Slit1 and Slit3 (Itoh et al., 1998) were cloned in into pSectagB (Invitrogen), and hSlit2 was previously described (Brose et al., 1999). Targeted mutagenesis for rat Robo1 and mouse and zebrafish Robo3A.1 was done using the QuikChange II XL Site –Directed Mutagenesis Kit (Agilent Technologies). The following forward and reverse specific mutagenic primers were used to generate rRobo1$^{N88P/K90R}$ (5'-GAA CCC GCC ACC CTC CCC TGT AGA GCT GAA GGC CGC CC-3') (5'-GGG CGG CCT TCA GCT CTA CAG GGG AGG GTG GCG GGT TC-3'), rRobo1^{N88P} (5-'GAA CCC GCC ACC CTC CCC TGT AAA GCT GAA GGC CGC CC-3') (5'- GGG CGG CCT TCA GCT TTA CAG GGG AGG GTG GCG GGT TC-3'), rRobo1^{K90R} (5'- GAA CCC GCC ACC CTC AAC TGT AGA GCT GAA GGC CGC CC-3') (5'- GGG CGG CCT TCA GCT CTA CAG TTG AGG GTG GCG GGT TC-3'), for rRobo1^{L130P} (5'-GGA TCT TTA TTT TTC CCA CGC ATA GTG CAT GG-3') (5'-CCA TGC ACT ATG CGT GGG AAA AAT AAA GAT CC-3'), mRobo3A.1^{P126L} (5'-CTG CCC AGC GGC GCC CTC TTC TTT CTC CGC ATT GTG CAC GGG CGT-

3') (5'-ACG CCC GTG CAC AAT GCG GAG AAA GAA GAG GGC GCC GCT GGG CAG-3'),), zRobo3a.1^{N83P} (5´- GAG CCT GCA ACT TTG CCC TGT AAG GCC GAA GG-3´) (5´- CCT TCG GCC TTA CAG GGC AAA GTT GCA GGC TC-3´), zRobo3a.1$^{N83P/K85R}$ (5´- GAG CCT GCA ACT TTG CCC TGT AGA GCC GAA GGA CGA CCG-3´) (5´- CGG TCG TCC TTC GGC TCT ACA GGG CAA AGT TGC AGG CTC-3´), zRobo3a.1^{L125P} (5´- GCT CCC TCT TCT TTC CCC GAA TTG TTC ACG G-3´) (5´- CCG TGA ACA ATT CGG GGA AAG AAG AGG GAG C-3´), xRobo3a.1^{N85P}(5´-AAC CAG CTA CTT TAC CCT GCA AAG CAG AAG G-3´) (5´-CCT TCT GCT TTG CAG GGT AAA GTA GCT GGT T-3´), xRobo3a.1^{L127P}(5´-GGC TCA CTT TTC TTT CCA CGA ATT GTT CAT GGC-3´) (5´-GCC ATG AAC AAT TCG TGG AAA GAA AAG TGA GCC-3´), mRobo3-Y1002F (5'-GCA GGA ATC TCC CTG TTC TTG GCT CAG ACT G-3') (5'-CAG TCT GAG CCA AGA ACA GGG AGA TTC CTG C-3'), Robo3-Y1019F (5'-GGT GAG GGT CCTGTC TTC AGC ACC ATT GAC-3') (5'-GTC AAT GGT GCT GAA GAC AGG ACC CTC ACC-3'). c-Src wild type and dominant-negative (K295M) GFP-fusion constructs were a kind gift from Olivier Destaing (University of Grenoble, France) and subcloned from pEGFP-N1 into the EcoRI-NotI site of pCX using Clontech's In-Fusion HD Cloning Kit (Clontech Ref: 011614) according to the manufacturer's instructions. Thermocycling conditions were programmed according to the manufacturer's instruction. All constructs were fully sequenced for accuracy.

For mutated mouse Robo3A.1^{P84N}, the sequence containing the mutation was synthesized and inserted in pCX-mRobo3A.1-V5-His using KpnI and SacI sites, full length chick Robo3A.1 (sequence from Ensembl ENSAMXP00000003239.1) was cloned into pCX using EcoRI site, full length

Xenopus tropicalis Robo3A.1 (sequence from Ensembl ENSXETT00000008543) and mutated *Xenopus tropicalis* Robo3A.1$^{N85P/K87R/L127P}$ DNA were cloned into pCX using AgeI site (GeneCust, Dudelange, Luxembourg). Mutated mouse Robo3A.1$^{P84N/R86K/P126L}$ DNA were synthesized and cloned into EcoRI site of the pCX vector (Genewiz, South Plainfield, New Jersey). HA-tagged intracellular domain of mouse Robo3.1 (R3-IC-HA; amino acid G907 to R1402 were cloned into the pCAGGS vector. mRobo3-ΔCC2-3 and mRobo3-ΔCC3 were derived by PCR from mRobo3A1. DCCΔP3 was derived by PCR from hDCC. Primers for mRobo3-ΔCC2-3 were as followed, 5'-CAAC ATG CTG CGC TAC CTG CTT AAA ACA C-3', forward, and 5'-CTC TTC CCC TAC TGG GTC AAT GGT-3', reverse. For mRobo3-ΔCC3, primers were 5'- CAAC ATG CTG CGC TAC CTG CTT AAA ACA C-3', forward, 5'- CCC CTC CGG ACA GCT CAG CTC ACA-3', reverse. For hDCCΔP3 primers were 5'-CACC ATG GAG AAT AGT CTT AGA TGT GTT TGG-3', forward and 5'-AGA CAA AAG TGG TGT GTA AGG GAC-3', reverse. Thermocycling conditions were programmed as follows: 1 min initial denaturation at 92 C; 20 cycles of denaturation (92 C, 45 sec), annealing at primer-specific temperatures (58 C, 45 sec), and extension (72 C, 20min); and a final extension step at 72 C for 10min. Product size was verified by electrophoresis on a 1% agarose gel. The resulting PCR fragments were cloned into the pcDNA3.1 expression vector using the pcDNA 3.1 Directional TOPO expression kit (Invitrogen) according to manufacturer's instruction.

For *in utero* electroporation, full-length V5-His-tagged mouse Robo3A.1 and full-length myc-tagged zebrafish Robo3A.1 (from pDestTol2pA2CMVrobo3a1myc vector, see below) were cloned into pCX-

GFP vector replacing the sequence for GFP, resulting in pCX-mRobo3A.1-V5-His and pCX-zRobo3A.1-myc respectively. To generate human and mouse Netrin-1 Alkaline Phosphatase fusion proteins in C-terminal, human and mouse Netrin-1 cDNAs were amplified by PCR and cloned in pAP-Tag-5 (GeneHunter, No.Q202) between Nhe1 and Bgl2 sites. Plasmids encoding human Netrin-1 and mouse Netrin-1 were provided by Dr Patrick Mehlen (Lyon, France).

Zebrafish expression constructs were generated by site-specific recombination-based cloning (multiside Gateway technology, Invitrogen) using the Tol2kit (http://tol2kit.genetics.utah.edu/index.php/Main_Page). Full length coding sequence of zebrafish *robo2* was amplified using (5´-GGG GAC AAG TTT GTA CAA AAA AGC AGG CTC CAT GGG TCC TTT AAC ACA CCT TTT-3´) (5´- GGG GAC CAC TTT GTA CAA GAA AGC TGG GTA TAA CTC TCC GGA AAA CTG CG-3´) from adult zebrafish brain cDNA introducing Gateway compatible attB1 and attB2 sites by PCR. Derived PCR product was then recombined into pDONR221 using BP clonase reaction to yield *pME-robo2.* *pDestTol2pA2;CMV:robo3a1myc*, *pDestTol2pA2;CMV:robo3a1*^{N83P}*myc, pDestTol2pA2;CMV:robo3a1*^{L125P}*myc* , *pDestTol2pA2;CMV:robo3a1*$^{N83P/K85R/L125P}$*myc* *and* *pDestTol2pA2;CMV:robo2myc* were generated by recombining either pME-*robo3a1*, pME-*robo3a1*^{N83P}*, pME-robo3a1*^{L125P}*, pME-robo3a1* $^{N83P/K85R/L125P}$ *or pME-robo2 with p5E-CMV/SP6*, *p3E-MTpA* and *pDEStTol2pA2* using LR clonase reaction according to manufacturers instructions. All clones were sequenced to verify inserts.

Fish maintenance, generation and staining of transgenic zebrafish strains

Zebrafish were maintained at 28.5 °C. To inhibit pigmentation, embryos were incubated in 0,2 mM phenylthiourea. Embryos were fixed in 4 % paraformaldehyde in PBS. For generation of stable transgenic lines 25 pg of either *hsp70l:zrobo3a.1p2Atdtomatocaax*, *hsp70l:zrobo3a.1*^{L125P}*p2Atdtomatocaax* or *hsp70l:zrobo3a.1*^{N83PK85RL126P}*p2Atdtomatocaax* plasmid and 30 pg Tol2 transposase RNA (*pCS2FA-transposase*; (Kwan et al., 2007) were co-injected into one-cell stage embryos. The following transgenic lines have been established *hsp70l:robo3a.1p2Atdtomatocaax*^{m1384} (*hsp70l:zrobo3a.1*), *hsp70l:robo3a.1*^{L125P}*p2Atdtomatocaax*^{m1385} (*hsp70l:zrobo3a.1*^{L125P}) and *hsp70l:robo3a.1*^{N83PK85RL126P}*p2Atdtomatocaax*^{m1386} (*hsp70l:zrobo3a.1*^{N83PK85RL126P}). For gain of function experiments transgenic fish were crossed to ABTL wild type fish. Mis-expression was induced by incubating the embryos at 39°C for 45 min. After heat shock treatment embryos were incubated at 28.5 °C until 72 hpf. Transgenic embryos were identified by the expression of TdTomato four hours after the heat shock treatment and sorted.

Whole mount immunohistochemistry on zebrafish embryos was performed as described previously (Holzschuh et al., 2003). Mauthner axons (MA) were visualized using the 3A10 antibody (obtained from the Development Studies Hybridoma Bank as supernatant) visualizing neurofilament. After immunohistochemistry, embryos were cleared in graded glycerol series. MA axon midline crossing was then inspected using a fluorescent

stereomicroscope (MZ16F, Leica) or a confocal microscope (LSM510, Zeiss). Midline crossing of MA axons was scored into the following categories: (I) wild type, (II) extra crossing events or (III) failure of midline crossing of one or both MA axons.

Generation of Slit -AP fusion proteins

The human Leucine Rich Repeat 2 (LRR2) Slit1/2-alkaline phosphatase (AP) (hSlit1-D2-AP or hSlit2-D2-AP) and the hSlit2N-AP (Ig domain1 to end of fifth EGF repeat) fusion proteins were previously described (Fouquet et al., 2007; Wang et al., 1999). For generating the hSlit3-D2-AP, the sequence encoding the second LRR of human *Slit3* (encoding amino acids 238-510) was amplified by PCR and cloned between the XhoI and XbaI sites of pAP-Tag-5 vector. Zebrafish Slit2-D2-AP (encoding amino acids 264-488) and chick Slit2-D2-AP (encoding amino acids 272-504) were cloned into the XhoI and XbaI sites in APTag5 (GeneCust, Dudelange, Luxembourg). Xenopus Slit2-D2-AP(encoding amino acids 271-506) was amplified by PCR from full-length xenopus Slit2 (Li et al., 1999) and cloned between XhoI and XbaI sites of pAP-Tag-5 vector.

In situ hybridization

Antisense riboprobes were labeled with digoxigenin-11-d-UTP (Roche Diagnostics, Indianapolis, IN) as described elsewhere (Marillat et al., 2002), by *in vitro* transcription of cDNA encoding mouse *Barhl1* (Li et al., 2004) or zebrafish *Robo3* (Schweitzer et al., 2013). Whole-mount embryos were

hybridized with digoxigenin-labeled riboprobes as described elsewhere (Marillat et al., 2004).

Identification of candidate kinases

To identify the kinase involved in Robo3 phosphorylation, we took advantage of two different bioinformatic tools covering either databases listing the mere presence of published literature-derived phospho-motifs (PhosphoMotif Finder; Amanchy et al., 2007) or more specifically artificial neural network predictions of kinase-specific phosphorylation sites in eukaryotic proteins (NetPhosK; Blom et al., 1999). The implementation of NetPhosK allowed us to screen the Robo3 cytoplasmic domain taking into account so called "sequence logos", most often conforming with accepted consensus sequence motifs of target sites unique to each kinase. Additionally, NetPhosK improves prediction specificity by evaluating phosphorylation sites using the "evoluationary-stable-site" procedure, revealing conservation of the acceptor residues identified and thus the likelihood of physiological relevance.

Surface biotinylation on hindbrain tissue and transfected cell lines

Hindbrain E14.5 tissue were dissected in ice cold Gey's balanced salt solution (Sigma) supplemented with 1% Glucose. Meninges were removed and pooled together with the residual tissue. Hindbrain surface was then rinsed with glass-Pasteur pipette to dislodge superficial pontine neurons and hindbrain was manually cut with micro-scalpel in approximately 1mm pieces. Tissue was spun down quickly and incubated with 1ml biotinylation reagent (Thermo Fisher/Pierce Kit for Cell Surface Protein Isolation) for 3 hours at 4°C on an

overhead shaker. Tissue was then washed 3x with ice cold TBS and lysed in 100μl lysis buffer followed by incubation on overhead shaker at 4°C for 45min. Tissue was spun down for 2min at 10.000xg. An aliquot was taken for total lysate fraction. Supernatant was incubated for 2.5h with Neutravidin beads (100μl of original stock, 50%slurry) previously equilibrated in wash buffer. After incubation, beads were washed 3x in 800μl wash buffer then once in 1xPBS. Beads were teluted in 20μl 2x Laemmli +DTT and loaded on a 50μl well gel. For Robo1 and Robo3 cell surface experiments, COS-7 cells were transfected with different expression vectors for 48 hr then the surface biotinylation was done according to the manufacturer's instructions (Thermo Fisher/Pierce Kit for Cell Surface Protein Isolation).

Cell culture, immunoprecipitation and Western blotting.

COS-7 cells (cell line from african green monkey kidney, SV40 transformed) (Sigma) were cultured in DMEM-Glutamax, supplemented with 10% fetal bovine serum (FBS) and 1% non-essential amino acids (NEAA, all from Invitrogen) and maintained at 37°C, 5% CO2. Cells were passaged at sub-confluency and cell batch was exchanged after a maximum of 11 passages. For phosphorylation studies, cells were transfected with various expression vectors 16-24 hours after plating using Lipofectamine 2000 according to the manufacturer's instructions (Invitrogen). In the evening of the following day, cells were starved in DMEM-Glutamax containing no supplements and cultured in the absence of serum for 12 hours to reduce basal phosphorylation of receptors. The next day, conditioned medium was removed and cells were re-starved in DMEM-Glutamax for 1.5 hours. For stimulation, cells were

incubated in DMEM-Glutamax containing 250ng/ml carrier-free recombinant mouse Slit2 (R&D systems, reference 5444-SL) or 250ng/ml recombinant human Netrin1-Fc (Adipogen / Coger, reference AG-40B-0075-C010) for 10min at 37°C.

P19 mouse teratocarcinoma cells were obtained from Sigma and cultured in DMEM/F12 (1:1) supplemented with 10% fetal bovine serum (FBS) and 1% non-essential amino acids (NEAA) (all Invitrogen, besides F12 from Sigma) and maintained at 37°C, 5% CO2 for basal conditions. For neuronal differentiation, cells were induced with 500nM all-trans retinoic acid (RA) (Sigma) in DMEM/F12 (1:1) supplemented with Insulin-Transferrin-Sodium-Selenite (ITS) (Sigma) for 48h, with the RA treatment being refreshed after 24h. RA induction leads to aggregation of cells and subsequent neurite extension observable after 48h. For the final differentiation, RA was withdrawn and the cells culture for an additional 24h before Netrin-1 stimulation. If applicable, cells were pretreated with 1μM PP2 for 30min (Sigma), 0.5μM LckI for 60min (Sigma) or 20μM GNF2 for 60min (Sigma) prior to stimulation with 250ng/ml recombinant human Netrin1-Fc (Adipogen / Coger, reference AG-40B-0075-C010) for 10min at 37°C in the presence of the respective inhibitors. Cells were processed for Immunoblotting as described below.

The Netrin-1 stimulation reaction was stopped by placing the cells on ice, quickly removing the stimulation mix and immediately adding NP-40 lysis buffer (10mM HEPES pH 7, 100 mM NaCl, 2 mM EDTA, 0.5% NP-40) supplemented with protease inhibitor cocktail and phosphatase inhibitor cocktail 1, 2 and 3 (Sigma) to the plate. The lysate was incubated at 4 °C for 20 min. After centrifugation at 14,000g for 10 min, the following antibodies

were added to the supernatants for 1 hour at 4°C: goat anti-human Robo3 (R&D Systems) for all mouse Robo3 expression constructs and mouse anti-c-myc (9E10; sc-40, Santa Cruz) for all others. Complexes were then incubated with Protein-G Sepharose Fast-Flow (Sigma) for an additional hour at 4°C. Subsequently, complexes were washed three times with cold lysis buffer and one time with 1x PBS prior to boiling in Laemmli SDS protein sample buffer. For Western blotting, samples were separated on 4-15% Mini- Protean TGX Tris-Glycine-buffer SDS-PAGE and transferred onto 0.2µm Trans-Blot Turbo nitrocellulose membranes (both from Biorad). Membranes were blocked for one hour at room temperature in 1xTBS (10mM Tris pH 8.0, 150 mM NaCl,) supplemented with 5%(w/v) dried skim milk powder or 5% BSA for phospho-epitope antibodies respectively. Primary antibody incubation was carried out overnight at 4°C, with the following antibodies: mouse anti-c-myc (9E10; sc-40, Santa Cruz) and mouse anti-pTyr (PY99; sc-7020, Santa Cruz), both at a dilution of 1:200.

A goat anti-mouse-HRP coupled secondary antibody was used for detection (Jackson ImmunoResearch, West Grove, PA). In between and after antibody incubations, membranes were extensively washed in TBS-T (TBS containing 2.5% Tween-20). Western blots were visualized using the enhanced chemiluminescence method (ECL prime Western Blotting detection reagent, Amersham). Western Blots were quantified using densitometric analysis (Image J) by normalizing phospho-signals to total protein levels for at least three independent experiments per case. Statistical significance was verified using the non-parametric Mann-Whitney test.

To verify protein expression levels of recombinant Robo3 in electroporated embryos, E16 hindbrains were dissected out in ice-cold Gey's balanced salt solution supplemented with 1% Glucose (Sigma). Tissue was then homogenized in lysis buffer (50mM TRIS pH 7.6, 1mM EDTA, 1% Triton-X 100) by passing 2-3 times through a 19G syringe. Incubation of samples for 45min on an overhead shaker at 4°C ensured thorough lysis. Lysates were spun down for 20min at 14,000g and the supernatant was incubated with mouse anti-c-myc antibody (9E10; sc-40, Santa Cruz) or mouse anti-V5 antibody (Invitrogen) overnight at 4°C. The following day, Protein-G Sepharose Fast-Flow beads (Sigma) were added and the sample was incubated for an additional hour at 4°C. Prior to Western blotting, beads were washed 4 times in 150mM Tris pH 7.6, 150mM NaCl. The samples were then processed for immunoblotting as described above. For the Robo3/DCC interaction experiments, HEK293 cells were transfected with various expression vectors using Lipofectamine 2000 according to the manufacturer's protocol (Invitrogen). After 48 hr, cells were lysed with Nint buffer supplemented with protease inhibitor cocktail and phosphatase inhibitor cocktail. In some experiments, the cells were serum-starved and then stimulated with mouse Slit-2 or human Netrin1-Fc and lysed. The lysate was incubated at 4°C for 20 min. After centrifugation at 14,000g for 10 min, supernatants were incubated for 2 hr at 4°C with the following antibodies: mouse anti-c-myc (9E10; Santa Cruz), rabbit anti-HA (Sigma), goat anti-hRobo3 (R&D systems), mouse anti-V5 (Invitrogen). Complexes were incubated Protein-G Sepharose Fast-Flow beads (Sigma) for 1 hr at 4°C. Subsequently, complexes were washed with cold lysis buffer and boiled in

Laemmli SDS protein sample buffer. The samples were then processed for migration, transfer and visualized as described above using goat anti-mouse, donkey anti-goat or goat anti-rabbit HRP (Jackson ImmunoResearch, West Grove, PA) as secondary antibodies and ECL Western Blotting detection reagent (Amersham).

Measurement of bound AP/binding affinity

COS-7 cells were incubated with different dilutions of hSlit2-D2-AP for 90 minutes at 37°C. After 2 washes with HBSS pH 7.0 containing 0.5 mg/ml BSA, 0.05% sodium azide and 20 mM HEPES, and 4 washes in PBS pH7.4, COS-7 cells were lysed in 10 mM Tris, pH8.0, 1% Triton X-100. The cell lysates were incubated at 65°C for 10 minutes and spun at 10,000g for 10 min. The amount of bound AP was revealed by p-nitrophenylphosphate (Sigma P7998) and measured at OD 405 nm. Binding affinity was calculated using Graph Pad Prism software (GraphPad Software, La Jolla, USA).

In utero electroporation

In utero electroporation of PN neurons was performed as described previously (Kawauchi et al., 2006), with some modifications. Endotoxin free plasmid DNA of pCX-EGFP (1 μg/μL) (provided by Dr M. Okabe, Osaka University, Japan) alone or in combination with pCX-mRobo3A.1-V5-His (5 μg/μL), pCX-mRobo3A.1ΔCC2-CC3-V5-His (5μg/μL), pCX mRobo3A.1^{Y1019F} (5 μg/μL), or pCX-zRobo3A1-myc (5 μg/μL) was diluted in PBS containing 0.01% Fast-green. 1 μL of diluted DNA was injected with a glass micropipette into the fourth ventricle of E13.5 mouse embryo. Five electric pulses (45 V, 50 ms,

950 ms interval between pulses) were applied with CUY21EDIT or NEPA21 electroporators (NepaGene, Ichikawa, Japan) using 5 mm diameter electrodes (CUY650-5, Nepagene). Electroporated embryos were dissected at E16.5-E17.5 and processed for imaging.

Explant cultures

The rhombic lip explant cultures were performed as described before (Alcantara et al., 2000; Yee et al., 1999). In brief, the lower rhombic lip from E14 embryos was dissected out as a single piece and cut into 150-300 µm fragments with fine tungsten needles. Dorsal spinal cord (DSC) explants from E11.5 embryos were obtained as previously described (Keino-Masu et al., 1996). Rhombic lip explants were co-cultured for 48-72 hours at a distance (200-600 µm) from either E11.5 mouse floor plate, E11.5 DSC explant (negative control), aggregates of HEK 293 cells stably transfected with a construct encoding Netrin-1-(VI-V)-Fc (*24*), or aggregates of non-transfected HEK 293 cells. In all cases, explants were embedded in rat-tail collagen and cultured in DMEM/F12 (1:1) supplemented with L-glutamine, 1% D-glucose, 2% FBS (5% FBS for DSC) and penicillin/streptomycin (Invitrogen), in a 5% CO2, 95% humidity incubator at 37°C. Explants were fixed in 4% PFA. Migrating pontine neurons were identified by Hoechst staining or immunostaining with mouse anti-beta-III-tubulin (Covance, MMs-435P), rabbit anti-mouse Pax6 (Chemicon, AB5409) and rabbit anti-human Barhl1 (Sigma, HPA004809) antibodies. Some explants were also dissected from E14.5 mouse embryos electroporated with pCX-GFP into the rhombic lip directly

before the culture preparation (see above). DSC explants were visualized by immunostaining with mouse anti-neuronal ßIII-tubulin.

Statistical analysis of explant cultures

Netrin-1 promotes the exit of postmitotic migrating neurons associated with thick fascicles of neurites from the embryonic lower rhombic lip at E12-E14 (Alcantara et al., 2000; Yee et al., 1999). For rhombic lip cultures evaluation, we counted the number of pontine neuron bundles migrating out of the explant towards the source of Netrin-1 (cell aggregate or floor plate) for each explant. Pontine neurons were identified by expression of GFP or by immunostaining for pontine neuron markers Pax6, Barhl1 or Robo3. We also quantified percentages of “responding” and “non-responding” rhombic lip explants. “Non-responding” refers to explants with no stream of pontine neurons/neurites. In each set of experiments positive controls (E14.5 wild type rhombic lip explants co-cultured with source of Netrin-1 (either floor plate or Netrin-1-expressing cells) and negative controls (E14.5 wild type rhombic lip explants co-cultured with dorso-lateral spinal cord explant or aggregate of non-transfected HEK 293 cells) were included. Explant cultures from at least 5 independent experiments were blind evaluated by investigator without notion of experiment setup. Compiled data is expressed as SEM and statistical significance was calculated using student’s t-test.

For Netrin-1 induced DSC explant outgrowth, ßIII-tubulin immunostaining signaling was quantified using ImageJ software (Rasband WS, ImageJ, U.S. National Institutes of Health, Bethesda, MD; http://rsb.info.nih.gov/ij/, 1997–2009). Signal from the axonal area was normalized with signal from the center

cell mass region for each explant, and compiled data is expressed as mean and SEM. Statistical significance was calculated using 2 tailed unpaired t-test. The culture was repeated in 3 separate experiments and the results were also evaluated blind by an independent investigator.

Microscopy

Hindbrains were dissected in ice cold Gey's balanced salt solution supplemented with 1% Glucose (Sigma), flat-mounted, fixed in 4% PFA for 1 hour at RT, washed, immunostained as described above and imaged using a confocal microscope (FV1000, Olympus). Images were processed with Adobe Photoshop and ImageJ software.

For time-lapse imaging, explant cultures were transferred on the insert to a 37°C stage incubator chamber (Life imaging Service, Switzerland) adapted to an upright microscope (Leica, DM6000) and provided with constant gas flow (5% CO2, 10% air). Explants were imaged with a spinning disk confocal system with 491 nm excitation filter and a Coolsnap HQ2 CCD camera (all from Roper scientific). Images were acquired using 10x (NA = 0.3) or 20x (NA = 0.5) water immersion objectives. Z-series confocal images were collected at 3 µm interval every 5 min. Brightness and contrast were adjusted for each frame using Metamorph (version 7.6.5.0, Universal Imaging Corporation) or Adobe Photoshop (version CS4).

Supplemental Figures

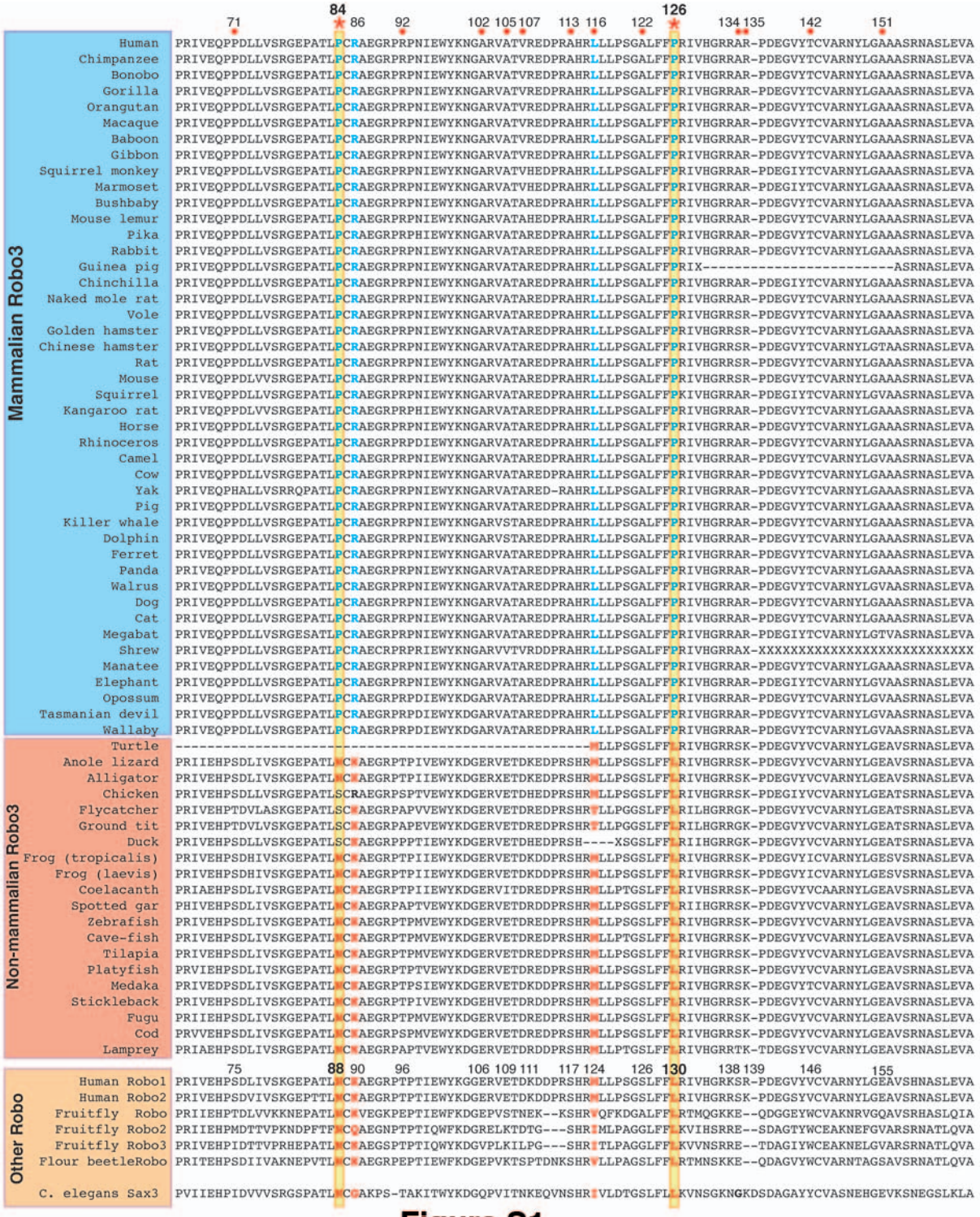
Mammalian Robo3
Non-mammalian Robo3
Other Robo
Human
Chimpanzee
Bonobo
Gorilla
Orangutan
Macaque
Baboon
Gibbon
Squirrel monkey
Marmoset
Bushbaby
Mouse lemur
Pika
Rabbit
Guinea pig
Chinchilla
Naked mole rat
Vole
Golden hamster
Chinese hamster
Rat
Mouse
Squirrel
Kangaroo rat
Horse
Rhinoceros
Camel
Cow
Yak
Pig
Killer whale
Dolphin
Ferret
Panda
Walrus
Dog
Cat
Megabat
Shrew
Manatee
Elephant
Opossum
Tasmanian devil
Wallaby
Turtle
Anole lizard
Alligator
Chicken
Flycatcher
Ground tit
Duck
Frog (tropicalis)
Frog (laevis)
Coelacanth
Spotted gar
Zebrafish
Cave-fish
Tilapia
Platyfish
Medaka
Stickleback
Fugu
Cod
Lamprey
Human Robo1
Human Robo2
Fruitfly Robo
Fruitfly Robo2
Fruitfly Robo3
Flour beetleRobo
C. elegans Sax3

Figure S1

Figure S1, related to Figure 1

Mammalian Robo3-Ig1 contains distinct amino acids when compared to other vertebrate Robo3 receptors.

Alignment of Robo3-Ig1 sequences. Robo3-Ig1 residues involved in Robo3-Slit2 binding and specific to mammals are presented in bold: mammalian specific residues are shown in blue, corresponding amino acids conserved in non-mammals and other Robos are shown in red. Non-conservative modifications are marked with a star and shown over yellow bands. Amino acids detected with a trace of positive selection in addition to Pro84 and Pro126 are presented with a red dot. Relative positions of these amino acids in human proteins are indicated for Robo3 (top) and Robo1 (bottom).

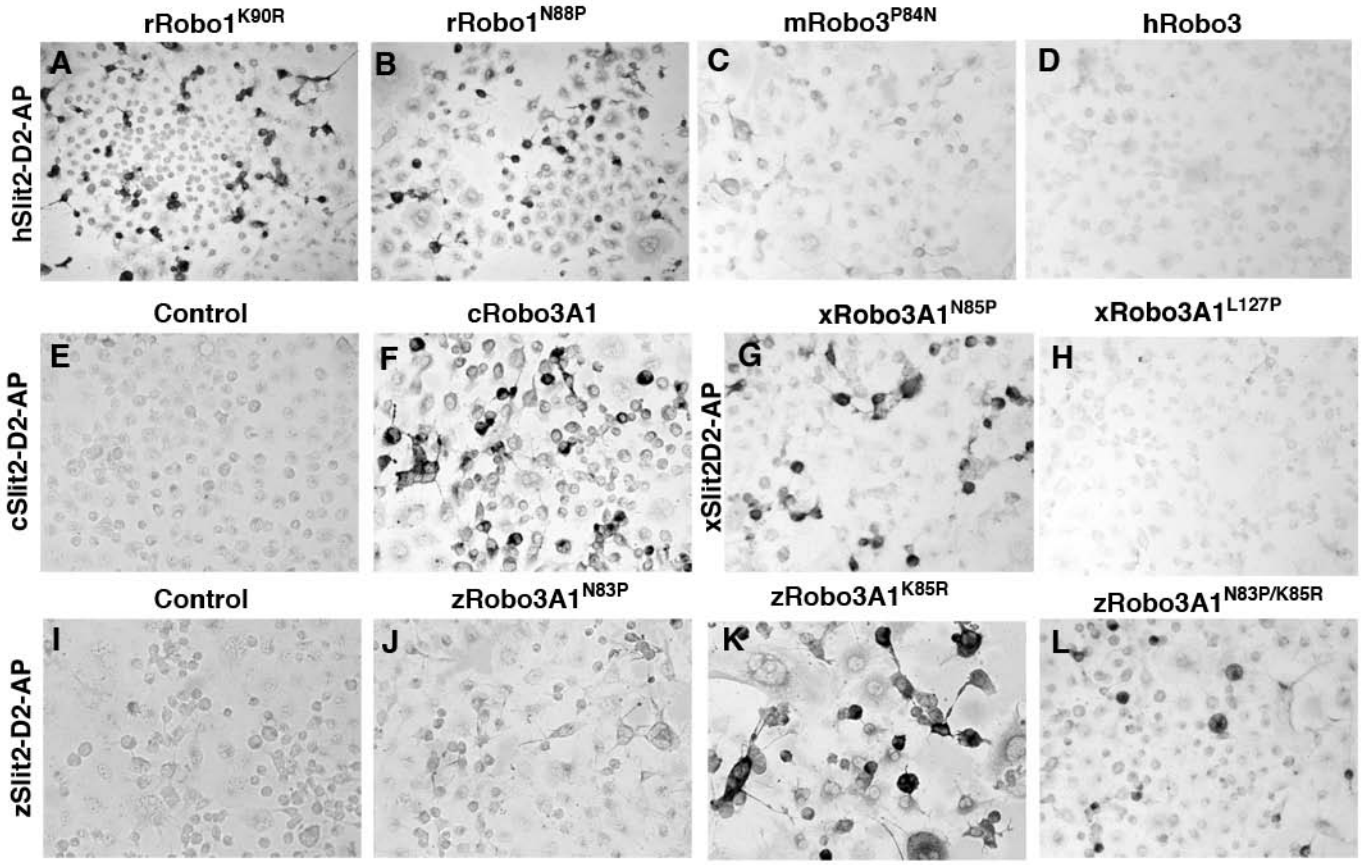
rRobo1K90R
rRobo1N88P
mRobo3P84N
hRobo3
hSlit2-D2-AP
A
B
C
D
Control
cRobo3A1
xRobo3A1N85P
xRobo3A1L127P
cSlit2-D2-AP
E
F
G
H
xSlit2D2-AP
Control
zRobo3A1N83P
zRobo3A1K85R
zRobo3A1N83P/K85R
zSlit2-D2-AP
I
J
K
L

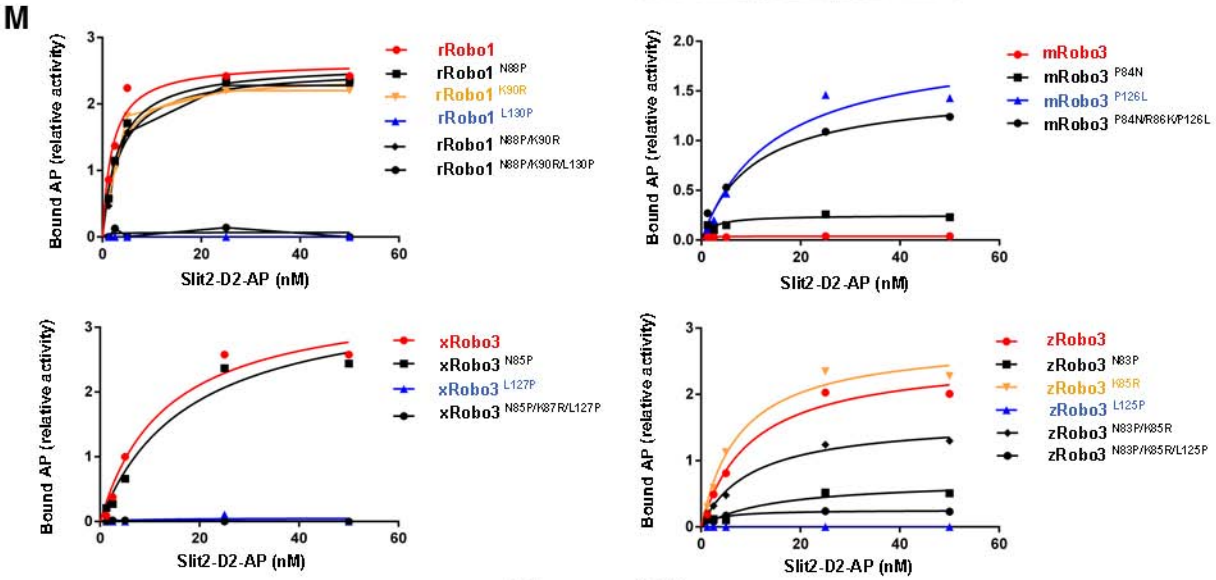
M
Bound AP (relative activity)
Slit2-D2-AP (nM)
rRobo1
rRobo1 N88P
rRobo1 K90R
rRobo1 L130P
rRobo1 N88P/K90R
rRobo1 N88P/K90R/L130P
mRobo3
mRobo3 P84N
mRobo3 P126L
mRobo3 P84N/R86K/P126L
xRobo3
xRobo3 N85P
xRobo3 L127P
xRobo3 N85P/K87R/L127P
zRobo3
zRobo3 N83P
zRobo3 N85R
zRobo3 L125P
zRobo3 N83P/K85R
zRobo3 N83P/K85R/L125P

Figure S2

Figure S2, related to Figure 2

Slit2 binding on mutant Robo1 and Robo3 receptors from various vertebrate species.

(A-D), hSlit2-D2-AP binds to COS cells expressing rRobo1^{K90R}, rRobo1^{N88P} but not mRobo3^{P84N} or hRobo3. (E, F) chicken Slit2-D2-AP binds to COS cells expressing cRobo3A.1. (G, H) xSlit2-D2-AP binds to Xenopus Robo3^{N85P} but does not bind to Robo3^{L127P}. (I-L) zebrafish Slit2-D2-AP binds to COS cells expressing zRobo3A.1^{K85R} but not zRobo3A.1^{N83P} or zRobo3A.1$^{N83P/K85R}$. (M) Scatchard analysis of hSlit2-D2-AP binding affinity to wild type and mutated Robo1 and Robo3 receptors. The data shown are representative of at least 3 independent experiments.

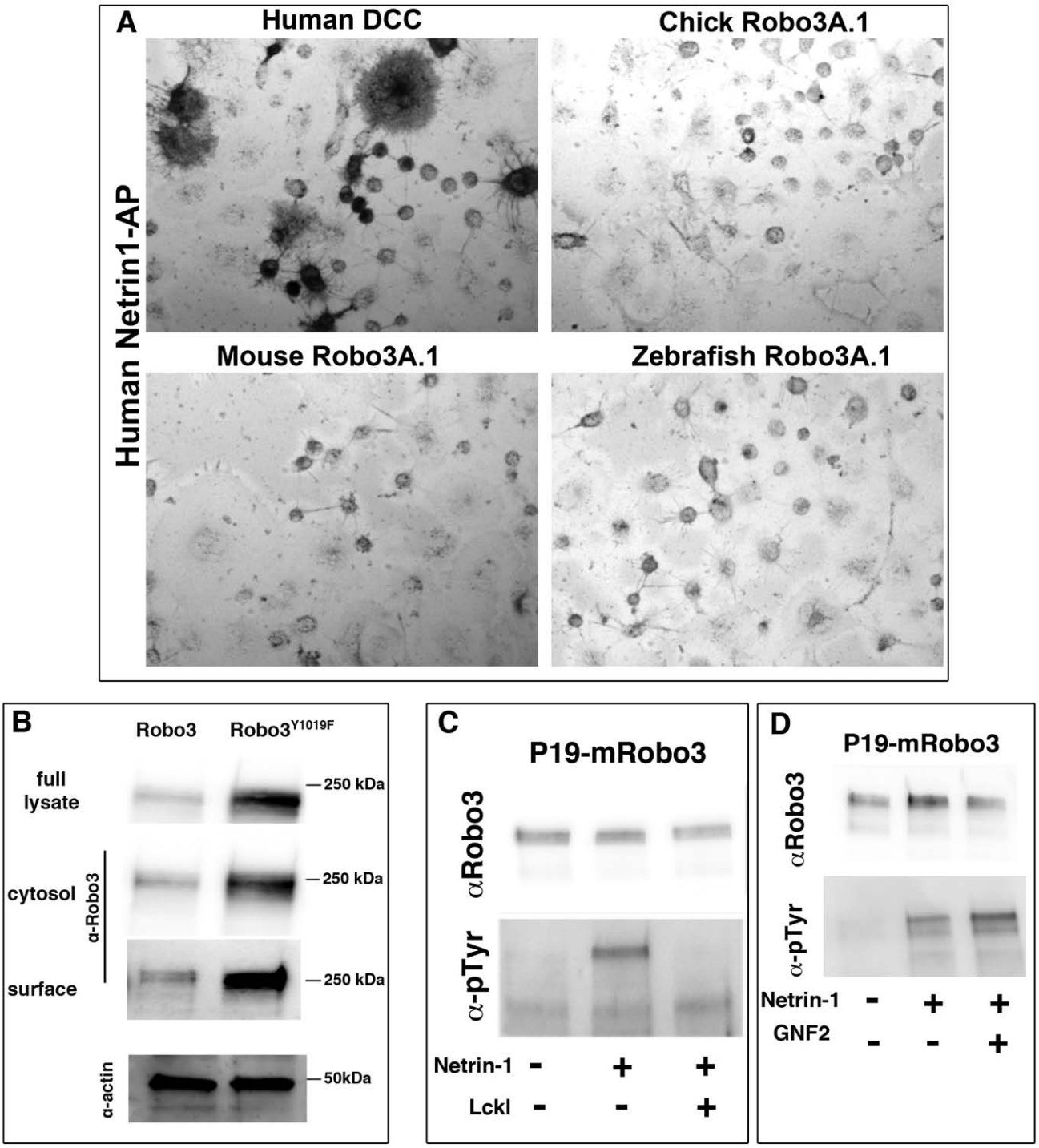
A
Human DCC
Chick Robo3A.1
Human Netrin1-AP
Mouse Robo3A.1
Zebrafish Robo3A.1
B
Robo3
Robo3Y1019F
full lysate
cytosol
surface
α-Robo3
250 kDa
250 kDa
250 kDa
α-actin
50kDa
C
P19-mRobo3
αRobo3
α-pTyr
Netrin-1 - + +
Lckl - - +
D
P19-mRobo3
αRobo3
α-pTyr
Netrin-1 - + +
GNF2 - - +

Figure S3

Figure S3, related to Figure 3

Lack of high-affinity binding of hNetrin-1 to mammalian or non-mammalian Robo3 and action of a Src-family kinase and c-Abl inhibitor. after hNetrin-1 stimulation (A) Human Netrin1-AP does not detectably bind COS cells expressing either mouse, zebrafish, chick Robo3A.1 while it binds its known receptor, human DCC, with high affinity. (B) Robo3Y1019F is normally expressed at the cell surface in transfected COS cells. (C) Lckl inhibits the tyrosine phosphorylation of endogenous Robo3 induced by Netrin-1 in P19 cells. (D) The allosteric c-Abl inhibitor GNF2 does not inhibit tyrosine phosphorylation of endogenous Robo3 after Netrin-1 stimulation in P19 cells.

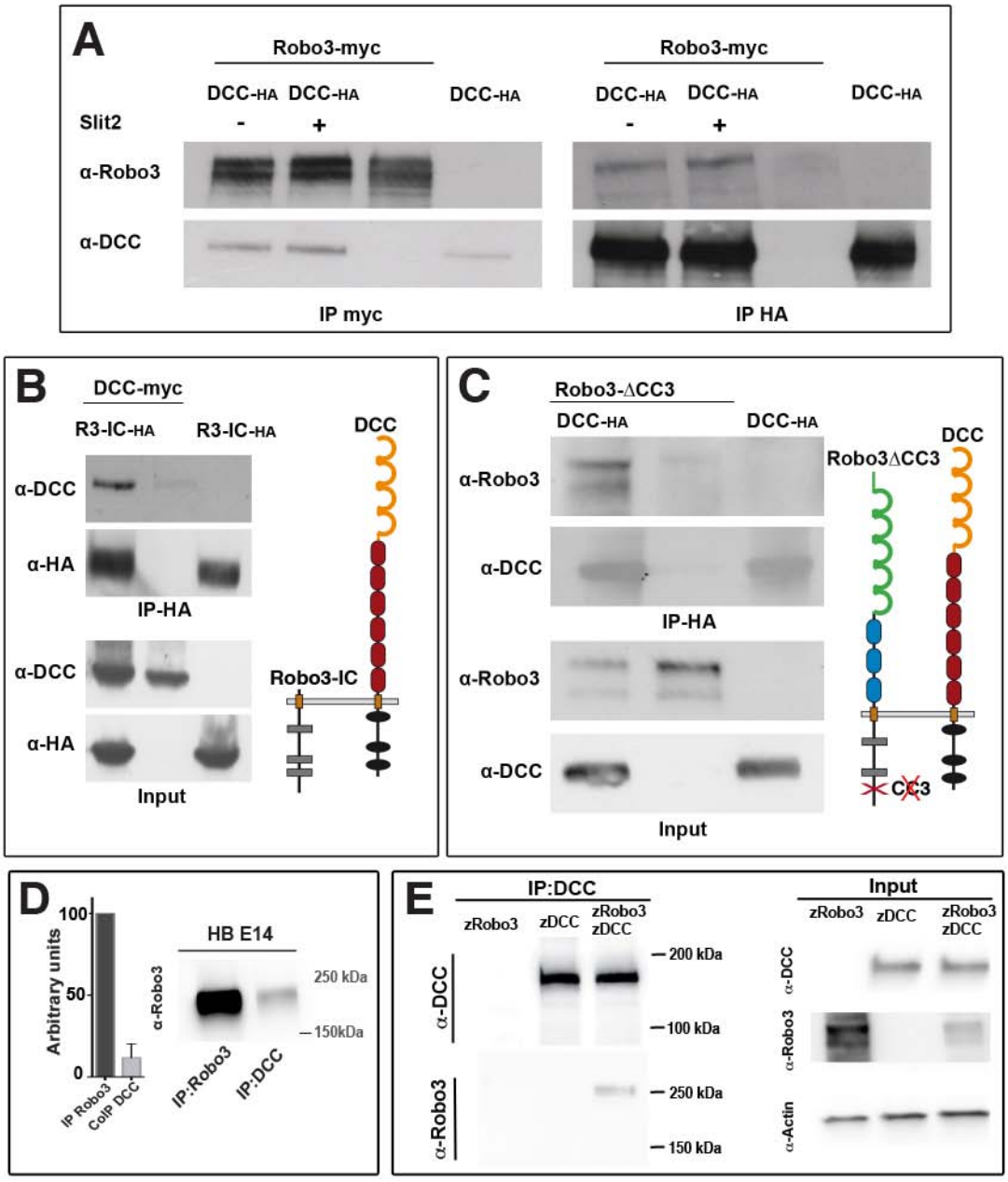
A
Robo3-myc
Robo3-myc
DCC-HA DCC-HA
DCC-HA
DCC-HA DCC-HA
DCC-HA
Slit2
-
+
-
+
α-Robo3
α-DCC
IP myc
IP HA
B
DCC-myc
R3-IC-HA
R3-IC-HA
DCC
α-DCC
α-HA
IP-HA
α-DCC
α-HA
Input
Robo3-IC
C
Robo3-ΔCC3
DCC-HA
DCC-HA
DCC
Robo3ΔCC3
α-Robo3
α-DCC
IP-HA
α-Robo3
α-DCC
Input
CC3
D
Arbitrary units
100
50
0
IP Robo3
CoIP DCC
HB E14
α-Robo3
250 kDa
150kDa
IP:Robo3
IP:DCC
E
IP:DCC
zRobo3
zDCC
zRobo3 zDCC
Input
zRobo3
zDCC
zRobo3 zDCC
α-DCC
α-Robo3
200 kDa
100 kDa
250 kDa
150 kDa
α-DCC
α-Robo3
α-Actin

Figure S4

Figure S4, related to Figure 4.

Robo3 and DCC interact *via* their intracellular domains.

(A) mRobo3A1-myc co-immunoprecipitates with hDCC-HA in HEK293 cells independently of Slit2. (B) DCC still interacts with a mutant form of Robo3 lacking the extracellular domain (Robo3-IC) or a Robo3 form deleted of the CC3 domain (C). (D) Robo3 and DCC were pulled down from E14.5 hindbrain protein extracts. The fraction of Robo3 that co-immunoprecipitates with DCC was calculated relatively to the total amount of Robo3 IP immunoprecipitated from the tissue extract, after western blotting using densitometric analysis (ImageJ). About 12% (± 3.8%, n=5) of Robo3 are in a complex with DCC. (E) zebrafish Robo3 co-immunoprecipitates with zebrafish DCC in HEK293 cells.

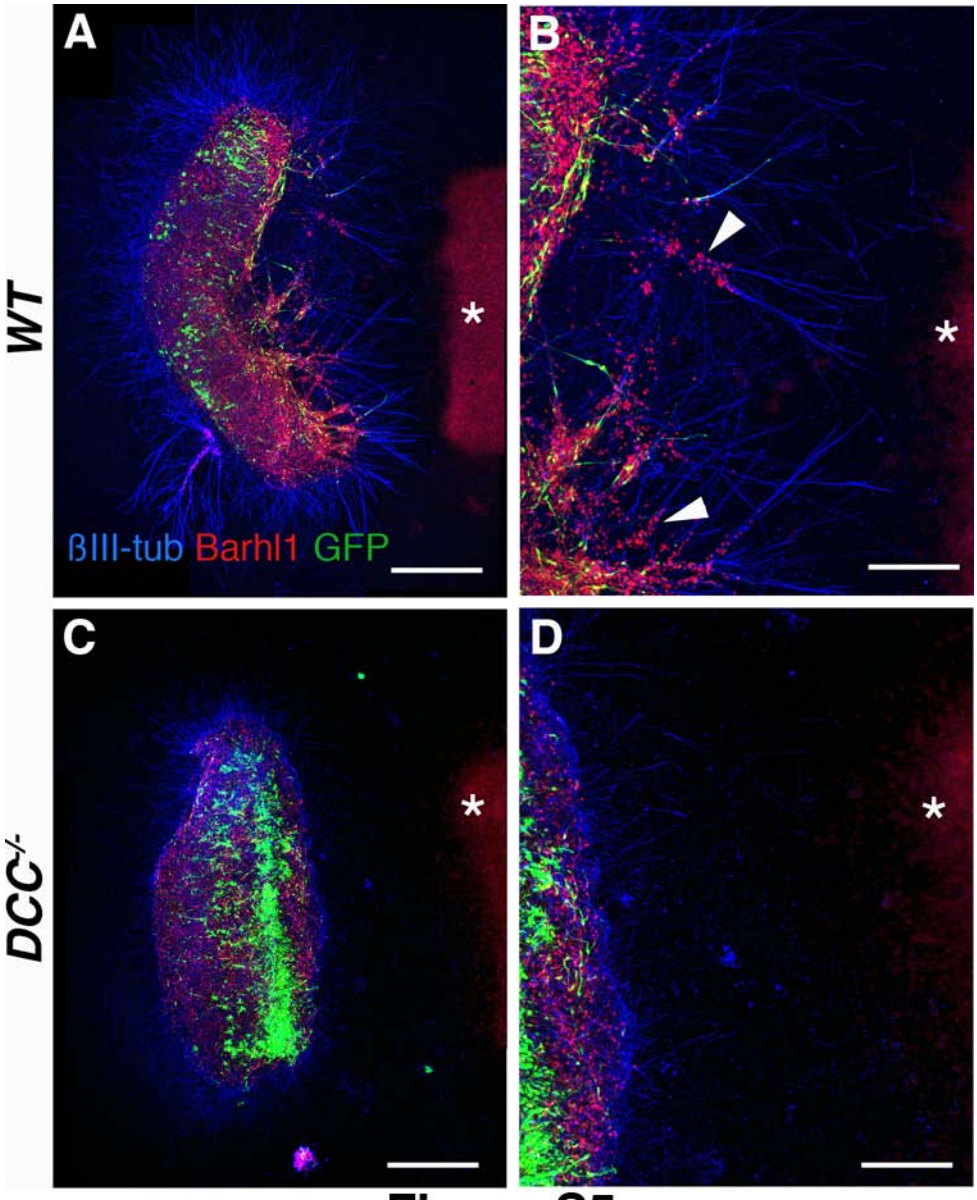

Figure S5

Figure S5, related to Figure 6

DCC$^{-/-}$ pontine neurons are not attracted by Netrin-1.

(A-D) Coculture in collagen gels of Netrin-1 expressing cells (asterisk) and E14.5 rhombic lip (rl) explants from wild type (A, B) or *DCC* KO (C, D) embryos. Explants were immunostained for Barhl1 and ßIII-tubulin. In wild type, streams of GFP+/Barhl1+ PN neurons (arrowheads in B) migrate out of the explants towards the Netrin-1 cell aggregate (arrowheads), whereas in *DCC* KO explants, GFP+/Barhl1+ neurons stay in the explant. See text for the quantification.

Scale bars: 450 µm in A, C; 200 µm in B, D.

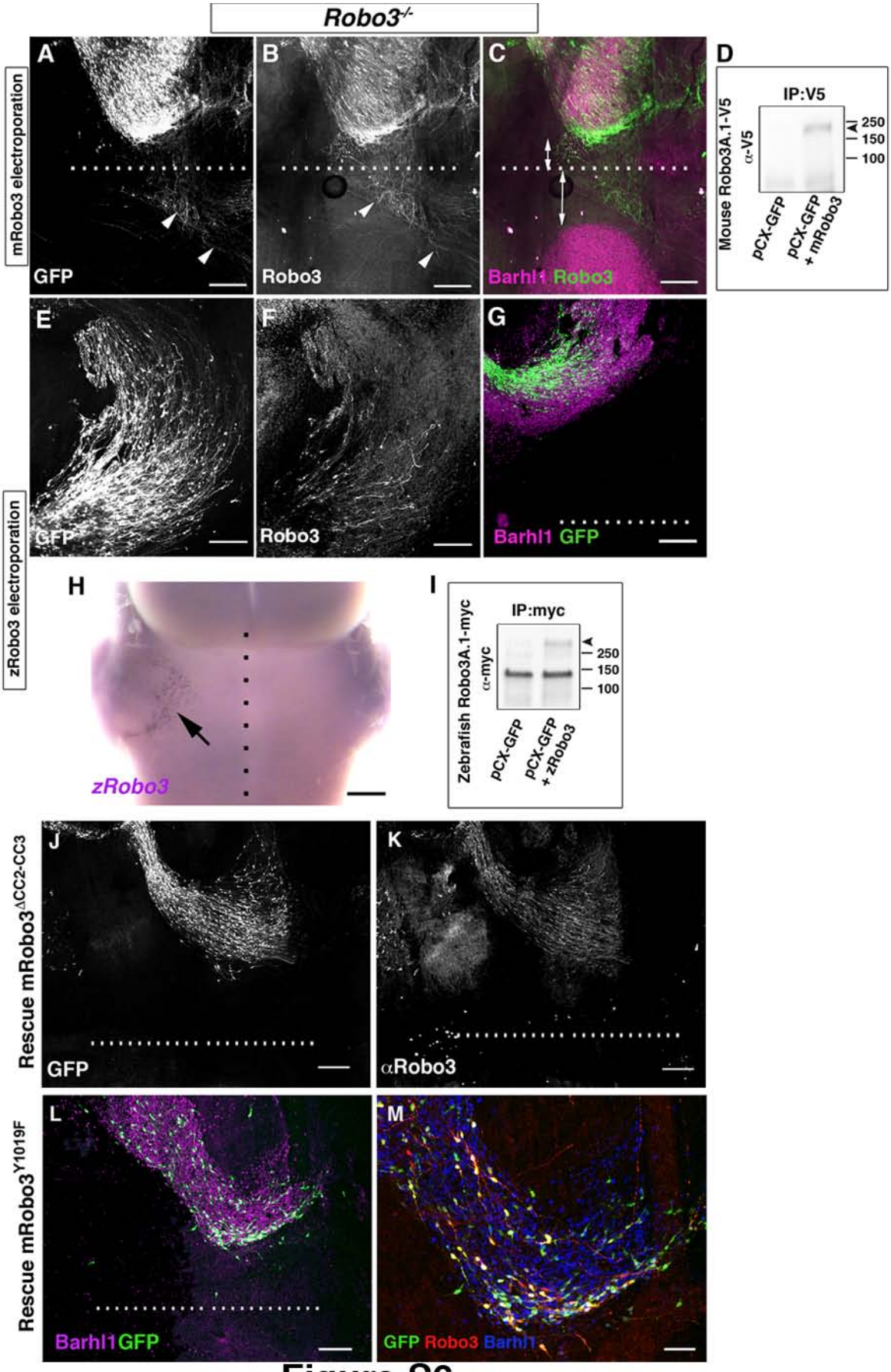
Robo3-/-
mRobo3 electroporation
zRobo3 electroporation
A
B
C
D
GFP
Robo3
Barhl1 Robo3
IP:V5
Mouse Robo3A.1-V5
α-V5
250
150
100
pCX-GFP
pCX-GFP + mRobo3
E
F
G
GFP
Robo3
Barhl1 GFP
H
I
zRobo3
IP:myc
Zebrafish Robo3A.1-myc
α-myc
250
150
100
pCX-GFP
pCX-GFP + zRobo3
Rescue mRobo3ΔCC2-CC3
J
K
GFP
αRobo3
Rescue mRobo3Y1019F
L
M
Barhl1 GFP
GFP Robo3 Barhl1

Figure S6

Figure S6, related to Figure 7.

Selective rescue of *Robo3*$^{-/-}$ pontine neurons by mammalian Robo3.

(A-D) E17.5 *Robo3*$^{-/-}$ hindbrain co-electroporated at E13.5 with mouse Robo3A.1 and GFP. Immunostaining for Robo3 (B) and for Barhl1/Robo3 (C). Electroporated pontine neurons send their axons (arrowheads) across the floor plate (dotted line in A-C). (C) The distance separating the floor plate from the front of migrating Barhl1 positive pontine neurons is reduced on the electroporated (rescued) side compared to the opposite (non-electroporated) side (double arrows). See text for quantification. (D) Expression levels of mRobo3A.1-V5 verified by immunoprecipitation from electroporated hindbrain protein extracts. (E-I) E17.5 *Robo3*$^{-/-}$ hindbrain co-electroporated at E13.5 with zebrafish Robo3A.1 and GFP. Immunostaining for Robo3 (F) and for Barhl1/GFP (G). Note that GFP/Robo3 positive neurons stay in the aberrant dorsal stream and do not approach the midline. (H) is a *Robo3*$^{-/-}$ embryo electroporated with zRobo3A.1 and processed as whole-mount for *in situ* hybridization with a zRobo3 probe. The arrows show zRobo3+ pontine neurons in the aberrant stream. (I) Expression levels of zRobo3A.1-myc (arrowhead) verified by immunoprecipitation from electroporated hindbrain protein extracts. (J, K) the mouse Robo3 lacking the CC2-CC3 domain fails to rescue ventral migration. (L, M) pontine neurons and axons from *Wnt1:cre;Robo3*$^{lox/lox}$ knockout embryo expressing Robo3^{Y1019F} phosphorylation mutant, failed to reach the midline. Scale bars: 60μm in (M), 100 μm in (A-C), 120 μm in (E and L) and (F), 150 μm in (G), 220 μm in (J, K), 400 μm in (H)

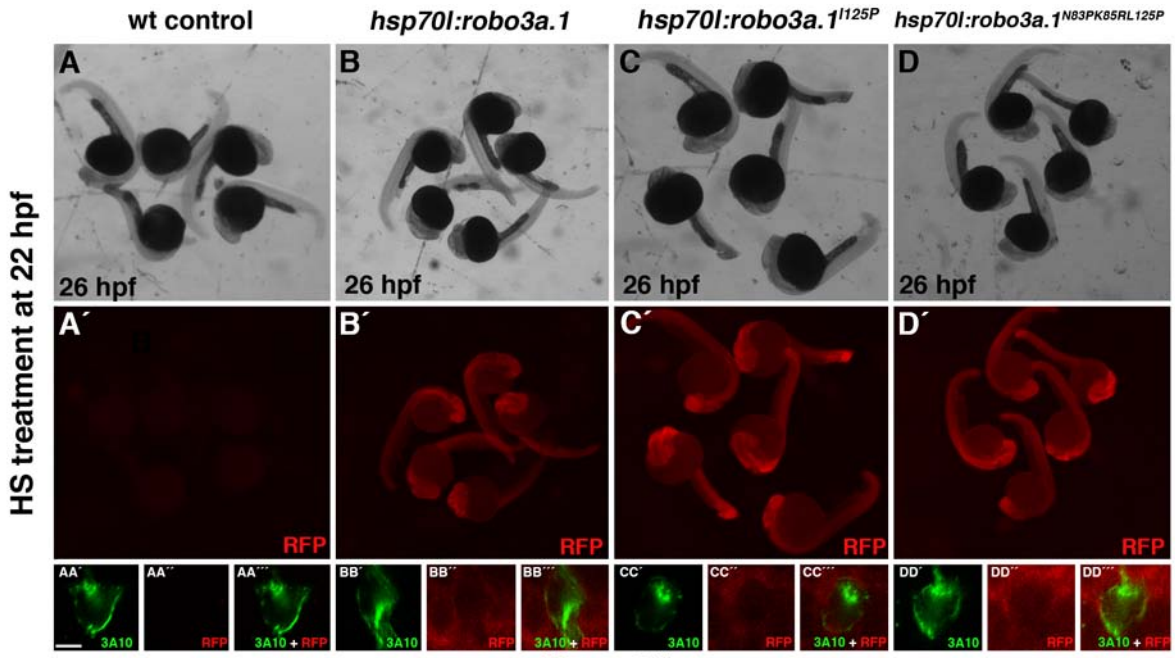
wt control
hsp70l:robo3a.1
hsp70l:robo3a.1^l125P
hsp70l:robo3a.1^N83PK85RL125P
HS treatment at 22 hpf
A
B
C
D
26 hpf
A´
B´
C´
D´
RFP
AA´
AA´´
AA´´´
BB´
BB´´
BB´´´
CC´
CC´´
CC´´´
DD´
DD´´
DD´´´
3A10
3A10 + RFP

Figure S7

Figure S7, related to Figure 7.

Characterization of transgenic heatshock zebrafish lines

(A-D´) Expression of Tdtomato as visualized by whole mount anti-RFP immunohistochemistry in control embryos and indicated transgenic lines upon heat shock treatment is shown. (AA´-DD´´´) High magnification of single confocal images (1 μm) is shown. Tdtomatocaax (labeled by anti-RFP antibody) is present in the cell membrane of MA neurons (labeled with 3A10 antibody). Scale bar in AA´ is 5μm.

Supplemental Movie S1, related to Figure 6.

Time-lapse video of *Robo3*$^{-/-}$ PN neurons expressing pCX-GFP in a RL explant cultured in collagen gel next to E11.5 floor plate. GFP+ neurons migrate inside the explant but do not leave it.

Supplementary Table S1, related to Figure 1.

Likelihood ratio tests (LRT) of positive selection in Robo proteins between the null model (neutrality) and the alternative model (positive selection).

Protein	Test	Likelihood of null model	Likelihood of alternative model	df	2*(ΔlnL)	Pvalue	Significant ?
Robo3	Model2 v Model 2null	-23444.569007	-23439.793159	1	9.551696	0.0025	YES
Robo1	Model2 v Model 2null	-24734.508243	-24733.991221	1	1.034044	0.25	NO
Robo2	Model2 v Model 2null	-14044.401341	-14043.648493	1	1.505696	0.2	NO

Supplementary Table S2, related to Figure 1.

List of amino acids found under positive selection with a Bayse Empirical Bayse > 0.5

Position in Human ROBO3	Amino acid	BEB posterior probability
71	P	0.589
84	**P**	**0.977**
92	R	0.821
102	A	0.582
105	A	0.708
107	V	0.603
113	A	0.624
116	L	0.513
122	A	0.609
126	**P**	**0.515**
134	A	0.972
135	R	0.826
142	T	0.789
151	A	0.564

Supplemental References

Alcantara, S., Ruiz, M., De Castro, F., Soriano, E., and Sotelo, C. (2000). Netrin 1 acts as an attractive or as a repulsive cue for distinct migrating neurons during the development of the cerebellar system. Development *127*, 1359-1372.

Amanchy, R., Periaswamy, B., Mathivanan, S., Reddy, R., Tattikota, S.G., and Pandey, A. (2007). A curated compendium of phosphorylation motifs. Nat Biotechnol *25*, 285-286.

Blom, N., Gammeltoft, S., and Brunak, S. (1999). Sequence and structure-based prediction of eukaryotic protein phosphorylation sites. Journal of molecular biology *294*, 1351-1362.

Brose, K., Bland, K.S., Wang, K.H., Arnott, D., Henzel, W., Goodman, C.S., Tessier-Lavigne, M., and Kidd, T. (1999). Slit proteins bind Robo receptors and have an evolutionarily conserved role in repulsive axon guidance. Cell *96*, 795-806.

Chen, Z., Gore, B.B., Long, H., Ma, L., and Tessier-Lavigne, M. (2008). Alternative splicing of the Robo3 axon guidance receptor governs the midline switch from attraction to repulsion. Neuron *58*, 325-332.

Fouquet, C., Di Meglio, T., Ma, L., Kawasaki, T., Long, H., Hirata, T., Tessier-Lavigne, M., Chedotal, A., and Nguyen-Ba-Charvet, K.T. (2007). Robo1 and robo2 control the development of the lateral olfactory tract. J Neurosci *27*, 3037-3045.

Holzschuh, J., Barrallo-Gimeno, A., Ettl, A.K., Durr, K., Knapik, E.W., and Driever, W. (2003). Noradrenergic neurons in the zebrafish hindbrain are induced by retinoic acid and require tfap2a for expression of the

neurotransmitter phenotype. Development *130*, 5741-5754.

Itoh, A., Miyabayashi, T., Ohno, M., and Sakano, S. (1998). Cloning and expressions of three mammalian homologues of Drosophila slit suggest possible roles for Slit in the formation and maintenance of the nervous system. Brain Res Mol Brain Res *62*, 175-186.

Kawauchi, D., Taniguchi, H., Watanabe, H., Saito, T., and Murakami, F. (2006). Direct visualization of nucleogenesis by precerebellar neurons: involvement of ventricle-directed, radial fibre-associated migration. Development *133*, 1113-1123.

Keino-Masu, K., Masu, M., Hinck, L., Leonardo, E.D., Chan, S.S., Culotti, J.G., and Tessier-Lavigne, M. (1996). Deleted in Colorectal Cancer (DCC) encodes a netrin receptor. Cell *87*, 175-185.

Kidd, T., Brose, K., Mitchell, K.J., Fetter, R.D., Tessier-Lavigne, M., Goodman, C.S., and Tear, G. (1998). Roundabout controls axon crossing of the CNS midline and defines a novel subfamily of evolutionarily conserved guidance receptors. Cell *92*, 205-215.

Kwan, K.M., Fujimoto, E., Grabher, C., Mangum, B.D., Hardy, M.E., Campbell, D.S., Parant, J.M., Yost, H.J., Kanki, J.P., and Chien, C.B. (2007). The Tol2kit: a multisite gateway-based construction kit for Tol2 transposon transgenesis constructs. Developmental dynamics : an official publication of the American Association of Anatomists *236*, 3088-3099.

Li, H.S., Chen, J.H., Wu, W., Fagaly, T., Zhou, L., Yuan, W., Dupuis, S., Jiang, Z.H., Nash, W., Gick, C*., et al.* (1999). Vertebrate slit, a secreted ligand for the transmembrane protein roundabout, is a repellent for olfactory bulb axons. Cell *96*, 807-818.

Li, S., Qiu, F., Xu, A., Price, S.M., and Xiang, M. (2004). Barhl1 regulates migration and survival of cerebellar granule cells by controlling expression of the neurotrophin-3 gene. J Neurosci *24*, 3104-3114.

Marillat, V., Cases, O., Nguyen-Ba-Charvet, K.T., Tessier-Lavigne, M., Sotelo, C., and Chedotal, A. (2002). Spatiotemporal expression patterns of slit and robo genes in the rat brain. J Comp Neurol *442*, 130-155.

Marillat, V., Sabatier, C., Failli, V., Matsunaga, E., Sotelo, C., Tessier-Lavigne, M., and Chedotal, A. (2004). The slit receptor Rig-1/Robo3 controls midline crossing by hindbrain precerebellar neurons and axons. Neuron *43*, 69-79.

Mille, F., Llambi, F., Guix, C., Delloye-Bourgeois, C., Guenebeaud, C., Castro-Obregon, S., Bredesen, D.E., Thibert, C., and Mehlen, P. (2009). Interfering with multimerization of netrin-1 receptors triggers tumor cell death. Cell Death Differ *16*, 1344-1351.

Sabatier, C., Plump, A.S., Le, M., Brose, K., Tamada, A., Murakami, F., Lee, E.Y., and Tessier-Lavigne, M. (2004). The divergent Robo family protein rig-1/Robo3 is a negative regulator of slit responsiveness required for midline crossing by commissural axons. Cell *117*, 157-169.

Schweitzer, J., Lohr, H., Bonkowsky, J.L., Hubscher, K., and Driever, W. (2013). Sim1a and Arnt2 contribute to hypothalamo-spinal axon guidance by regulating Robo2 activity via a Robo3-dependent mechanism. Development *140*, 93-106.

Wang, K.H., Brose, K., Arnott, D., Kidd, T., Goodman, C.S., Henzel, W., and Tessier-Lavigne, M. (1999). Biochemical purification of a mammalian slit protein as a positive regulator of sensory axon elongation and branching. Cell *96*, 771-784.

Yee, K.T., Simon, H.H., Tessier-Lavigne, M., and O'Leary, D.M. (1999). Extension of long leading processes and neuronal migration in the mammalian brain directed by the chemoattractant netrin-1. Neuron *24*, 607-622.

Name	*Latin name*	Accession number
Robo3		
American alligator	*Alligator mississippiensis*	XP_006258795.1
Anole lizard	*Anolis carolinensis*	XP_006035991.1
Baboon	*Papio anubis*	ENSACAP00000000366.3
Bonobo	*Pan paniscus*	XP_003910954.1
Bushbaby	*Otolemur garnettii*	XP_003819980.1
Camel	*Camelus ferus*	ENSOGAP00000014081.2
Cat	*Felis catus*	XP_006174427.1
Cave fish	*Astyanax mexicanus*	ENSFCAP00000006275.3
Chicken	*Gallus gallus*	ENSAMXP00000003239.1
Chimpanzee	*Pan troglodytes*	ENSGALP00000001377.4
Chinchilla	*Chinchilla lanigera*	ENSPTRP00000007574.4
Chinese alligator	*Alligator sinensis*	XP_005378502.1
Chinese hamster	*Cricetulus griseus*	XP_003515732.1
Cod	*Gadus morhua*	ENSGMOP00000001634.1
Coelacanthe	*Latimeria chalumnae*	ENSLACP00000012994.1
Cow	*Bos torus*	ENSBTAP00000005697.4
Dog	*Canis lupus familiaris*	ENSCAFP00000016381.3
Dolphin	*Tursiops truncatus*	ENSTTRP00000012567.1
Duck	*Anas platyrhynchos*	ENSAPLP00000012381.1
Elephant	*Loxodonta Africana*	ENSLAFP00000024352.1
Ferret	*Mustela putorio furo*	ENSMPUP00000006051.1
Flycatcher	*Ficedula albicolis*	ENSFALP00000005508.1
Fugu	*Takifugu rubipes*	ENSTRUP00000008702.1
Gibbon	*Nomascus leucogenys*	ENSNLEP00000009060.1
Golden hamster	*Mesocricetus auratus*	XP_005069292.1

Gorilla	*Gorilla gorilla*	ENSGGOP00000014773.2
Ground tit	*Pseudopodoces humilis*	XP_005528554.1
Guinea pig	*Cavia porcellus*	ENSCPOP00000000072.2
Horse	*Equus caballus*	ENSECAP00000011961.1
Human	*Homo sapiens*	ENSP00000380903.1
Kangaroo rat	*Dipodomys ordii*	ENSDORP00000010027.1
Killer whale	*Orcinus orca*	XP_004280756.1
Lamprey	*Petromyzon marinus*	ENSPMAP00000010521.1
Macaque	*Macaca mulatta*	ENSMMUP00000028413.2
Manatee	*Trichechus manatus*	XP_004379418.1
Marmoset	*Callithrix jacchus*	ENSCJAP00000014995.2
Medaka	*Oryzias latipes*	ENSORLP00000006664.1
Megabat	*Pteropus vampyrus*	ENSPVAP00000003156.1
Microbat	*Myotis lucifugus*	ENSMLUP00000016971.1
Mouse	*Mus musculus*	ENSMUSP00000034643.5
Mouse lemur	*Microcebus murinus*	ENSMICP00000001550.1
Naked mole rat	*Heterocephalus glaber*	XP_004874532.1
Opossum	*Monodelphis domestica*	ENSMODP00000004729.3
Orangutan	*Pongo abelii*	ENSPPYP00000004598.2
Painted turtle	*Chrysemys picta bellii*	XP_005294765.1
Panda	*Ailuropoda melanoleuca*	ENSAMEP00000000872.1
Pig	*Sus scrofa*	ENSSSCP00000016124.1
Pika	*Ochotona princeps*	ENSOPRP00000009522.1
Platyfish	*Xiphophorus maculatus*	ENSXMAP00000006176.1
Rabbit	*Oryctolagus cuniculus*	ENSOCUP00000023052.1
Rat	*Rattus norvegicus*	ENSRNOP00000060623.1
Rhinoceros	*Ceratotherium simum*	XP_004438482.1

Shrew	*Sorex araneus*	ENSSARP00000009204.1
Spotted gar	*Lepisosteus oculatus*	ENSLOCP00000006316.1
Squirrel	*Ictidomys tridecemlineatus*	ENSSTOP00000014587.2
Squirrel monkey	*Saimiri boliviensis*	XP_003923602.1
Stickleback	*Gasterosteus aculeatus*	ENSGACP00000026594.1
Tasmanian devil	*Sarcophilus harrisii*	ENSSHAP00000018216.1
Tilapia	*Oreochromis niloticus*	ENSONIP00000019865.1
Vole	*Microtus ochrogaster*	XP_005347519.1
Wallaby	*Macropus eugenii*	ENSMEUP00000007116.1
Walrus	*Odobenus rosmarus*	XP_004413768.1
Xenopus	*Xenopus tropicalis*	ENSXETP00000008543.3
Xenopus	*Xenopus laevis*	NP_001164069.1
Yak	*Bos mutus*	XP_005904012.1
Zebrafish	*Danio rerio*	ENSDARP00000027377.8
Robo2		
Chicken	*Gallus gallus*	AAK94294.1
Chimpanzee	*Pan troglodytes*	ENSPTRP00000026097.5
Chinese softshell turtle	*Pelodiscus sinensis*	ENSPSIP00000020214.1
Cod	*Gadus morhua*	ENSGMOP00000007743.1
Dog	*Canis lupus familiaris*	ENSCAFP00000011789.3
Fugu	*Takifugu rubipes*	ENSTRUP00000010208.1
Gorilla	*Gorilla gorilla*	ENSGGOP00000011507.2
Horse	*Equus caballus*	ENSECAP00000009128.1
Human	*Homo sapiens*	ENSP00000417335.2
Kangaroo rat	*Dipodomys ordii*	ENSDORP00000002275
Lesser hergehog tenrec	*Echinops telfairi*	ENSETEP00000000759
Macaque	*Macaca mulatta*	ENSMMUP00000016559

Marmoset	*Callithrix jacchus*	ENSCJAP00000000219.2
Medaka	*Oryzias latipes*	ENSORLP00000005129.1
Mouse	*Mus musculus*	ENSMUSP00000112776.1
Orangutan	*Pongo abelii*	ENSPPYP00000015242.2
Painted turtle	*Chrysemys picta bellii*	XP_005294686.1
Shrew	*Sorex araneus*	ENSSARP00000011336
Stickleback	*Gasterosteus aculeatus*	ENSGACP00000015054.1
Tetraodon	*Tetraodon nigroviridis*	ENSTNIP00000019343.1
Tilapia	*Oreochromis niloticus*	ENSONIP00000021275.1
Turkey	*Melagris gallopavo*	XP_003202908.1
Wallaby	*Macropus eugenii*	ENSMEUP00000008871
Xenopus	*Xenopus tropicalis*	ENSXETP00000045356.2
Xenopus	*Xenopus laevis*	ACZ99259.1
Robo1		
Chicken	*Gallus gallus*	ENSGALP00000024963.4
Chinese turtle	*Pelodiscus sinensis*	ENSPSIP00000008498.1
Chimpanzee	*Pan troglodytes*	ENSPTRT00000066780
Cod	*Gadus morhua*	ENSGMOP00000007707.1
Dog	*Canis lupus familiaris*	ENSCAFP00000011732.3
Elephant	*Loxodontha Africana*	ENSLAFP00000006431.4
Fugu	*Takifugu rubipes*	ENSTRUP00000013694.1
Gorilla	*Gorilla gorilla*	ENSGGOP00000001433.2
Ground tit	*Pseudopodoces humilis*	XP_005524257.1
Guinea pig	*Cavia porcelus*	ENSCPOP00000009012.2
Horse	*Equus caballus*	ENSECAP00000015937.1
Human	*Homo sapiens*	ENSP00000406043.2
Marmoset	*Callithrix jacchus*	ENSCJAP00000000293.2

Medaka	*Oryzias latipes*	ENSORLP00000005165.1
Mouse	*Mus musculus*	ENSMUSP00000023600.7
Opossum	*Monodelphis domestica*	ENSMODP00000021041.3
Orangutan	*Pongo abelii*	ENSPPYP00000015243.2
Platypus	*Ornithorhynchus anatinus*	XP_003430991.1
Tilapia	*Oreochromis niloticus*	ENSONIP00000021261.1
Wallaby	*Macropus eugenii*	ENSMEUP00000009380.1
Xenopus	*Xenopus tropicalis*	NP_001096171.1
Invertebrate Robo		
Fruitfly-Robo	*Drosophila melanogaster*	FBpp0071834.5
Fruitfly-Robo2	*Drosophila melanogaster*	AAG41425.1
Fruitfly-Robo3	*Drosophila melanogaster*	FBpp0077587.5
Flour beetle-Robo	*Tribolium castaneum*	AEZ54711.1
C.elegans-Sax3	*Caenorhabditis elegans*	ZK377.2b.1

Supplemental Table S3
Accession numbers of
the Robo sequences used for the study.